# IRF5 guides monocytes towards an inflammatory CD11c$^{+}$ macrophage phenotype and promotes intestinal inflammation

Alastair L. Corbin[1*], Maria Gomez-Vazquez[1*], Dorothée L. Berthold[1], Moustafa Attar[1], Isabelle C. Arnold[1,2], Fiona M. Powrie[1&], Stephen N. Sansom[1&†], Irina A. Udalova[1&†]

[1]The Kennedy Institute of Rheumatology, University of Oxford, Oxford. UK

[2]Institut für Molekulare Krebsforschung, University of Zurich, Zurich, Switzerland

[*] [&] These authors contributed equally to this work.

[†] Corresponding authors: irina.udalova@kennedy.ox.ac.uk (I.A.U);

stephen.sansom@kennedy.ox.ac.uk (S.N.S)

## One sentence summary

## The transcription factor IRF5 promotes macrophage differentiation in Helicobacter-driven intestinal inflammation in mice

## Abstract

Mononuclear phagocytes (MNPs) are vital for maintaining intestinal homeostasis but in response to acute microbial stimulation can also trigger immunopathology, accelerating recruitment of Ly6C$^{hi}$ monocytes to the gut. The regulators that control monocyte tissue adaptation in the gut remain poorly understood. Interferon Regulatory Factor 5 (IRF5) is a transcription factor previously shown to play a key role in maintaining the inflammatory phenotype of macrophages. Here we investigate the impact of IRF5 on the MNP system and physiology of the gut at homeostasis and during inflammation. We demonstrate that IRF5 deficiency has a limited impact on colon physiology at steady state but ameliorates immunopathology during *Helicobacter hepaticus* induced colitis. Inhibition of IRF5 activity in MNPs phenocopies global IRF5 deficiency. Using a combination of bone marrow chimera and single cell RNA-sequencing approaches we examined the intrinsic role of IRF5 in controlling colonic MNP development. We demonstrate that IRF5 promotes differentiation of Ly6C$^{hi}$ monocytes into CD11c$^{+}$ macrophages and controls the production of anti-microbial and inflammatory mediators by these cells. ~~We found IRF5 to play only a limited role in the MNP development at steady state, both in the gut and in the blood.~~ Thus, we identify IRF5 as a key transcriptional regulator of the colonic MNP system during intestinal inflammation.

## Introduction

The term Inflammatory Bowel Disease (IBD) encompasses a group of debilitating inflammatory conditions of the gastrointestinal tract that affects ~0.5-1% of westernised populations (*1*). The IBDs are associated with high morbidity and burden healthcare systems (*2, 3*). Conventional IBD therapies are limited by moderate-high rates of adverse events, or patient unresponsiveness, whilst approximately 40% of patients successfully treated with anti-TNFα become refractory to therapy (*2*). Therefore, there is unmet clinical need for IBD therapies. The aetiology of IBD is unknown, but interplay between host genetics, and environmental factors, and the microbiota contribute to disease pathogenesis (*1*).

Mononuclear Phagocytes (MNPs), including monocytes, macrophages, and Dendritic Cells (DCs), are present in large numbers in the colonic Lamina Propria (cLP), and carry out diverse, overlapping functions critical to the maintenance of intestinal homeostasis. The dysregulation of the intestinal MNP system leads to infection and inflammation (*4-11*).

The origins of the intestinal MNP systems has been the topic of considerable debate in recent years, clouded by inconsistent nomenclature and shared surface markers between macrophages and DCs. Intestinal Lamina Propria DCs at the steady state are largely derived from pre-DC precursors, generated in the bone marrow, which are understood differentiate into three major intestinal DC subsets. These subsets comprise an XCR1 positive ($Xcr1^{+}SIRP\alpha^{-}CD103^{+}Cd11b^{-}CX3CR1^{-}$) population that is analogous to classical dendritic cells (cDC) 1 DCs, and two cDC2-like SIRPα positive ($SIRP\alpha^{+}Xcr1^{-}$

Cd11b$^{+}$CX3XR1$^{+}$) subsets which can be further discriminated by CD103 expression(*12, 13*). In addition, the existence of a discrete population of hybrid macrophage/DC cells within the cDC2 intestinal compartment has been described (*14*). The ontogeny of intestinal DCs during inflammation is more complicated since some monocyte-derived cells may acquire phenotypic and functional DC hallmarks (*15-17*).

Intestinal Lamina Propria macrophages have dual origins: from embryonically derived macrophages (CD4$^{+}$ Tim4$^{+}$) that self-renew, and monocytes, but in the adult mouse, most of the macrophage turnover is of monocytic origin (*18, 19*). In mice, the differentiation of monocytes to macrophages in the cLP has been termed the “monocyte waterfall” (*19*). After entering the cLP, naïve Ly6C$^{hi}$, MCHII$^{-}$ (P1) monocytes begin maturing by acquiring expression of MHCII (P2) before downregulating Ly6C expression. The pool of MHCII$^{+}$ cells comprises of Ly6C$^{+/-}$CX3CR1$^{Int}$ monocyte/macrophage intermediates (P3) and fully mature Ly6C$^{-}$CX3CR1$^{hi}$F4/80$^{hi}$CD64$^{hi}$MHCII$^{hi}$ macrophages (P4) (*19, 20*). During infection, de novo recruited monocytes give rise to CD11c$^{+}$ intestinal macrophages that are phenotypically pro-inflammatory (*21*). The blood origin of intestinal macrophage subsets was also confirmed in human studies where two monocyte-derived macrophage populations: CD11c$^{+}$ with high turnover and CD11c$^{-}$ with slow turnover, were identified at steady state (*22*). It was suggested that CD11c$^{+}$ macrophages might be an intermediate between blood monocytes and tissue resident CD11c$^{-}$ macrophages (*22*).

The regulators that control the transition of monocytes through a number of intermediate differentiation states are largely unknown, but the cytokines, TGFβ and IL10, have been linked to the development of cLP tissue-resident macrophages (*23, 24*). CX$_3$CR1$^{IL10R-}$ mice exhibited heightened inflammation, which maintained a pro-inflammatory mono-

macrophage state, preventing their full differentiation and initiating spontaneous colitis (*24*). Loss of TGFβ-Receptor on macrophages resulted in a minor impairment of macrophage differentiation, defined by transcriptional profiling of monocyte to macrophage transition in the cLP (*23*).

One candidate intrinsic regulator of the intestinal macrophage signature is Interferon Regulatory Factor 5 (IRF5), which was described to promote an inflammatory macrophage phenotype(*25*) and has variants that are genetic risk factors for Ulcerative Colitis and Crohn's Disease (*26-28*). IRF5 is activated by phosphorylation and ubiquitination events downstream of Pattern Recognition Receptors (PRRs), e.g. NOD2, TLR2, and TLR4, and directly regulates many cytokines associated with IBD (IL-1β, IL-6, IL-10, IL-12, IL-23, TNF), placing IRF5 as a nexus for the regulation of inflammatory responses (*1, 25, 29*). To formally examine the role of IRF5 in the establishment of intestinal MNP system, we compared the continuum of cell states of wild type (WT) and IRF5 deficient (*Irf5*$^{-/-}$) MNPs at steady state and during *Helicobacter hepaticus* (*Hh*) induced intestinal inflammation using a combination of competitive Mixed Bone Marrow Chimaera (MBMC), single cell gene expression analysis (scRNA-seq) and functional validation approaches. *Hh* infection concomitant with the administration of anti-Interleukin 10 Receptor (αIL10R) antibodies triggers IL-23 dependent intestinal inflammation with robust $T_H1/T_H17$ T cell response, which carries many features of human IBD(*9, 30-32*). In this model, $CX_3CR^{int}$ and $CD11c^+$ monocyte/macrophages intermediates drive immunopathology by producing pro-inflammatory cytokines such as IL-23, IL-1β and TNFα (*9, 33*). We show that IRF5 promotes the differentiation of monocytes into a

bactericidal and inflammatory CD11c+ macrophage phenotype during *Hh* + αIL10R-induced colitis and is essential for the development of immunopathology in this model.

## Results

### IRF5 deficiency has limited impact on colon physiology at steady-state

In steady state, we found that the colons (**Fig.1A**) and caeca (**Supplementary Fig.S1A**) of WT and *Irf5*$^{-/-}$ were comparable in morphology. Sections were scored for epithelial hyperplasia, nucleated cell infiltrate, area affected, and submucosal oedema and displayed no obvious signs of inflammation (score < 3) and no morphological differences between WT and *Irf5*$^{-/-}$ (**Fig. 1B and Supplementary Fig S1B**). The immune compartment of the cLP was evaluated by flow cytometry and revealed that the number of leukocytes in the colon (live CD45$^{+}$) were comparable between WT and *Irf5*$^{-/-}$ (**Fig. 1C**).

Next, we assessed the levels of IRF5 expression in the cells of the colon and demonstrated that non-myeloid, and non-leukocyte populations expressed low levels of IRF5 compared to CD11b$^{+}$ myeloid cells (**Fig.1D).** Among myeloid cells, MNPs, i.e. monocytes, macrophages and DCs, expressed the highest levels of IRF5 (**Fig.1D).** The composition of the cLP myeloid compartment in WT and *Irf5*$^{-/-}$ was profiled using the gating strategy that included definition of the stages of monocyte differentiation(*9, 20*) (**Supplementary Fig.S1C**). Frequencies and absolute numbers of Ly6C$^{hi}$MHCII$^{-}$ (P1) and Ly6C$^{hi}$MHCII$^{+}$ (P2) monocytes and CD11b$^{+}$ DCs among the infiltrated leukocytes were similar in *Irf5*$^{-/-}$ animals but a higher frequency of F4/80$^{+}$ macrophages was observed in WT mice (5.1%) than in *Irf5*$^{-/-}$ (2.9%) (**Fig.1E, Supplementary Fig S1E**). IRF5-deficient and WT Ly6C$^{hi}$ MHC II$^{+}$ monocytes and macrophages were no different in their levels of apoptosis (**Fig. 1F**). Thus, we hypothesised that IRF5 may promote differentiation of monocytes to macrophages in the cLP.

**IRF5 deficiency protects against intestinal inflammation**

Next, we evaluated the effect of IRF5 deficiency on the pathogenesis of intestinal inflammation. WT and *Irf5*$^{-/-}$ mice were subjected to *Hh* + αIL10R colitis for 21 days and inflammatory indices were analysed upon sacrifice. Morphological analysis (**Fig 2A, Supplementary Fig. S2A**) and histological scoring indicated that both colons (**Fig. 2B**) and caeca (**Supplementary Fig. S2B**) were protected from colitis by IRF5-deficiency. The leukocyte infiltrate to the cLP was significantly reduced in *Irf5*$^{-/-}$ mice (**Fig. 2C**), consistent with the reduced levels of inflammation in the colon and caecum of *Irf5*$^{-/-}$ animals. Next, we profiled $T_H1$ and $T_H17$ lymphocyte responses that are involved in the pathogenesis of colitis (*34*). *Irf5*$^{-/-}$ mice displayed a significantly reduced $T_H1$ effector response as quantified by emergence of IFNγ$^+$ CD4$^+$ T cells, and a non-significant reduction in the number of IL-17a$^+$ $T_H17$ cells and double positive IFNγ$^+$/IL-17a$^+$ cells (**Fig. 2D**).

*Hh* + αIL10R colitis in WT mice led to splenomegaly, but not in *Irf5*$^{-/-}$ mice (**Fig. 2E**), indicating that they were also protected from systemic aspects of disease. Despite the altered immune response, *Hh* presence in the caecal faeces were unaffected in *Irf5*$^{-/-}$ compared to WT, quantified by detection of the *Hh* Cytolethal Distending Toxin B (cdtB) gene (**Supplementary Fig. S2C**), ruling out differential bacterial colonisation in WT and IRF5-deficient animals.

Myeloid cells make up a significant part of the leukocyte pool at the peak of inflammation in the colon(*33*). Ly6C$^{hi}$ monocytes are rapidly recruited to the gut in response to inflammatory signals, with Ly6C$^{hi}$MHCII$^+$ inflammatory monocytes becoming the predominant cells that carry out inflammatory effector functions (*9, 15, 16, 20, 24, 35, 36*).

Indeed, we observed an increase in the frequency of Ly6C$^{hi}$MHCII$^{+}$ inflammatory monocytes (0.9% to 2.2%) at the peak of *Hh* + αIL10R induced inflammation, while the frequency of F4/80$^{+}$ macrophages diminished (**Figs 2F and 1E; Supplementary Fig. S2D**). The frequencies of the DC populations remained unaffected by ongoing inflammation (**Figs 2F and 1E**). IRF5 deficiency significantly attenuated the predominance of Ly6C$^{hi}$MHCII$^{+}$ inflammatory monocytes **(Fig. 2F**), approximating the monocyte-macrophage waterfall observed at the steady state (**Fig. 1F**). At the peak of inflammation all MNP populations in *Irf5*$^{-/-}$ animals were smaller in absolute numbers than those of their wildtype counterparts (**Supplementary Fig S2E**). Finally, to confirm that IRF5 activity in MNPs is a major contributor into the immunopathology of intestinal inflammation, we subjected Cx3cr1$^{cre}$xIRF5$^{flox/flox}$ animals, which are deficient in IRF5 specifically in their MNP compartment (**Supplementary Fig S2E**), to the *Hh* + αIL10R colitis model. Histological scoring indicated that both the colons (**Fig. 2G, H**) and caeca (**Supplementary Fig S2F, E**) of these animals were protected from colitis by IRF5-deficiency in MNPs.

These data demonstrate that IRF5 plays a critical role in the pathogenesis of intestinal inflammation via the MNP system.

**IRF5 has limited effect on monocyte development in the bone marrow and blood**

At homeostasis, a higher frequency of fully differentiated F4/80$^{+}$ macrophages was observed in WT compared to *Irf5*$^{-/-}$ mice (**Fig 1**), suggesting that IRF5 may play role in monocyte differentiation. However, in *Hh* + aIL10R induced colitis, the different

inflammatory environments between WT and *Irf5*$^{-/-}$ animals obscured this effect (**Fig 2**). To compare the differentiation competence of WT and *Irf5*$^{-/-}$ monocytes in a shared environment, we performed mixed bone marrow chimera experiments. The lethally irradiated mice were reconstituted with 50:50 WT:*Irf5*$^{-/-}$ bone marrow mix and the efficiency of reconstitution in the bone marrow, of blood monocytes, and of the cLP MNP compartment were investigated. We observed no difference in reconstitution of long term (LT)- or short term (ST)- haematopoietic stem cells (HSCs), myeloid progenitors (common myeloid progenitors (CMPs), granulocyte-monocyte progenitors (GMP) and megakaryocyte-erythrocyte progenitors (MEP) or Ly6C$^{hi}$ mature monocyte population in the bone marrow (**Supplementary Fig S3A, B**). IRF5 expression assessed by intracellular staining using flow cytometry was negligible in LT-HSCs, ST-HSCs, and CMPs but detectable in GMPs and MEPs. Ly6C$^{hi}$ monocytes express the highest levels of IRF5 among the tested progenitor and mature cell populations (**Supplementary Fig. S3C**). The reconstitution of Ly6C$^{hi}$ monocytes in the blood was not affected by IRF5 deficiency, but more Ly6C$^{lo}$ monocytes appeared to be derived from WT progenitors (**Supplementary Fig. S3D**).

To further investigate an impact of IRF5 deficiency on the composition and phenotype of monocytes in the blood in non-inflammatory conditions, we conducted single cell RNA-sequencing (scRNA-seq) analysis of CX3CR1$^{+}$ WT and *Irf5*$^{-/-}$ cells from five mixed bone marrow chimeras. We identified five subpopulations of cells (**Supplementary Fig. 4A**) that included discrete sets of *Ly6c2*$^{hi}$, *Cd36*$^{hi}$, *Cd74*$^{hi}$ and *Cd74*$^{hi}$/*Cd209*$^{hi}$ cells similar to those reported previously(*37*), (**Supplementary Fig. 4C**). As would be expected for immature monocytes, the set of *Ly6c2*$^{hi}$ cells (Cluster I) also showed high expression of

*Sell* and *Ccr2* (**Supplementary Fig 4D).** Two clusters of Ly6c$^{lo}$ Cd36$^{+ve}$ cells (Clusters II & III) were also positive for the transcription factors *Cebpb* and *Nr4a1* which are known to regulate the transition from Ly6c$^{hi}$ to Ly6c$^{lo}$ monocytes(*37*) (**Supplementary Fig 4D).** Of these, the largest (Cluster II) was distinguished by high expression of *Itgal*, while the smaller (Cluster III) showed high expression of *Apoe* (**Supplementary Fig 4C**). The remaining two clusters (IV and V) both expressed *Cd74* and *Ccr2*, with the smallest cluster (V) also showing expression of *Cd209a*, *Ciita, Batf3* and *H2-Dmb1* suggestive of a monocyte-derived DC (moDC) precursor phenotype(*38*) (**Supplementary Fig 4D**). Overall, we found broadly similar proportions of WT and Irf5$^{-/-}$ in the different clusters, although, consistent with the FACS data (**Supplementary Fig S3D**), the knockout did show a small decrease in *Cd36$^{hi}$* (47.2% *Irf5$^{-/-}$* vs 55.7% WT) together with a concomitant increase in *Ly6c2$^{hi}$* (32.6% Irf5$^{-/-}$ vs 26.1% WT) cell frequency relative to WT (**Supplementary Fig 4B)**. The transcriptional phenotypes of the *Irf5$^{-/-}$* and WT cells were highly similar within each of the clusters. In total only 8 genes (including *Irf5*) were found to be significantly differentially expressed ($|fc| > 1.5$, BH adjusted p value $< 0.05$, Wilcoxon tests), with nearly all of the differences being identified in the putative moDC precursor population (**Supplementary Fig 6A**). Together, these data indicate that although IRF5 is unlikely to have a global impact on monocyte development and phenotypes in the bone marrow and blood, it may help to promote the transition of blood monocytes from *Ly6C$^{hi}$* to *Ly6C$^{lo}$/Cd36$^{hi}$* and play a role in shaping the development of *Cd74$^{hi}$/Cd209$^{hi}$* moDCs.

**IRF5 has subtle effect on CD11c+ intestinal macrophages at steady state**

Under homeostatic conditions Ly6C$^{hi}$ monocytes continuously extravasate into the colon where they give rise to heterogenous populations of macrophages (*13*). Because a change in this process may affect susceptibility to colitis we investigated whether IRF5 can act in a cell-intrinsic fashion to regulate the composition of MNP pools in the steady-state cLP. While the reconstitution of Ly6C$^{hi}$ monocytes in the blood was not affected by IRF5 deficiency, more Ly6C$^{hi}$ monocytes in the cLP were derived from WT progenitors (**Supplementary Fig. S3E**). This finding is consistent with the previously reported more efficient recruitment of donor WT than *Irf5*$^{-/-}$ monocytes into the tissue in mixed bone marrow chimera (*39*). Next, we performed scRNA-seq analysis of *Cx3cr1*$^{+ve}$ MNP extracted from the cLP of the steady state WT/*Irf5*$^{-/-}$ mixed bone marrow chimera. We identified ten distinct subpopulations (**Fig 3A and Supplementary Fig 5**) that comprised *Cd209a*$^{+ve}$ dendritic cells (cluster 10), *Clec4a*$^{+}$ and *Ly6c2*$^{hi}$ monocytes (clusters 8 and 9) and seven *Adgre1*$^{+ve}$ (encoding for F4/80) macrophage populations (clusters 1-7) (**Fig 3A)**. As expected, the Mϕ clusters represented the majority of MNPs in uninfected mixed bone marrow chimera, consistent with the FACS-based analysis (**Fig 1E and Fig S6C**). The Mϕ broadly split into two compartments that were distinguished by expression of *Itgax* (*Cd11c*) and *Mrc1* (*Cd206*) (orange and red ellipses **Fig 3A**). The *Cd11c* Mϕ also showed expression *Cd9* and *Acp5* and comprised separate populations of *Hes1*$^{+ve}$ and *Il7r*$^{+ve}$/*Il10*$^{+ve}$ cells that may represent epithelial associated and resident tolerogenic Mϕ populations respectively (*33, 40*) (**Fig 3D**). Macrophages with high expression of *Mrc1* also showed higher expression of *Alox5ap* and the anti-inflammatory molecule *Ifitm3* (*41*) (**Fig 3E**). Subpopulations of the *Mrc1* Mϕ were characterised by high expression of key monocyte chemo-attractants *Ccl8* (*42*) and *Ccl2* (which encode the ligand for CCR2).

Orthogonal to groupings by *Cd11c* vs *Mrc1* status the Mϕ showed differences in the expression of *Runx3* and *Cx3cr1* which are associated with mature macrophages (**Fig 3F**). While surface expression of CX3CR1 protein is known to be associated with maturity, *Cx3cr1* gene expression was higher in *Runx3*$^{-ve}$ cells suggesting that transcription of this gene is down-regulated as Mϕ mature. Additionally, both the *Cd11c* and *Mrc1* Mϕ populations exhibited apparent differences in activation state being split between expression of *Klf2*, which is known to inhibit the pro-inflammatory activation of immune cells(*43*) and expression of genes associated with Mϕ activation such as the key NF-κB target gene *Rel* and the *Nlrp3* inflammasome (**Fig 3F**). No *Timd4* (Tim-4) expression was detected in any of the macrophage clusters (data not shown), indicating that, as expected, the monocyte-independent resident macrophage population was not represented amongst the donor-derived cells(*18*). Overall the distribution of WT and Irf5$^{-/-}$ cells between the clusters was similar (**Fig 3B)** although there were fewer *Irf5*$^{-/-}$ (25.2%) than WT (32.1%) cells in the activated *Cd11c* Mϕ (clusters 1 and 6). In contrast, there was an increase in the frequency of DCs (4.0% vs 1.6%) and *Clec4e*$^{+ve}$ monocytes (cluster 8; 7.4% vs 4.3%) amongst the *Irf5*$^{-/-}$ cells. Across the clusters only 34 genes were significantly affected ($|fc| > 1.5$, BH adjusted p value $< 0.05$, Wilcoxon tests) by the lack of IRF5, with the majority of differences (n=23) being observed in the DC cluster (**Supplementary Fig 6B**). However, amongst the *Cd11c*$^{+ve}$ macrophage clusters 1, 3, and 6 we did note a consistent down-regulation of *Ccl4* (also known as Macrophage inflammatory protein-1β, Mip-1β) in the *Irf5*$^{-/-}$ cells (**Supplementary Fig 6B**).

Altogether absence of the IRF5 had a subtle effect on the composition and phenotype of the steady state colonic lamina propria MNP compartment that was suggestive of a role for IRF5 in controlling *CD11c*+ MNP development.

**IRF5 promotes generation of CD11c+ macrophages in inflamed colon**

Next we subjected $CX_3CR1^+$ WT and *Irf5*$^{-/-}$ MNPs isolated from the inflamed cLP of three *Hh* + αIL10R MBMCs to scRNA-seq analysis **(Supplementary Fig. S7A)**. Examination of the top cluster markers genes (**Supplementary Fig. S7B**) revealed the existence of two groups of monocytes, two clusters of macrophages and four clusters of dendritic cells (**Fig. 4A**). The monocyte clusters comprised a set of *Ly6c2*-high immature monocytes ("*Ly6c* Mono") and a group of mature monocytes ("*MHCII* Mono") that expressed MHCII genes such as *H2-Ab1* and the pro-inflammatory cytokine *Il1b* (**Fig. 4B**). The two macrophage clusters were clearly demarcated by expression of *Adgre1* (*F4/80)*, *Cd81* and *Cx3cr1.* The largest cluster of *Cd11c* Mϕ was characterised by the high expression level of *Itgax* (*Cd11c*) and known cLP macrophage markers, such as MHC glycoproteins (*H2-M2*), complement molecules (*C1qa*,*b*,*c)*, tetraspanins (*Cd63*, *Cd72, Cd81*), oxidative stress response (*Hebp1*) and anti-microbial molecules (*Lyz2*, *Acp5, Dnase1l3*) (**Fig. 4B** and **Supplementary Fig. S7B**). The second cluster of *Cd206* Mϕ lacked *Itgax* expression but was defined by high expression of *Mrc1* (*Cd206*), chemokines (e.g. *Ccl2, Ccl3*, *Ccl4*, *Ccl7, Ccl8, Ccl12, Cxcl2)*, scavenger, phagocytic and immunoactivating receptors (*Cd36, Fcgr4, Clec4b1*) and anti-viral molecules (*Ch25h, Gbp2b*) (**Fig. 4B** and **Supplementary Fig. S7B**). The remaining four clusters of cells lacked *Cd64* expression and showed expression of established dendritic cell markers such as *Flt3*, *Cd11c*, and the *Ciita*-

dependent DC-specific MHCII genes *H2-DMb2* and *H2-Oa*(*44*). "*Sirpa* DC i" and "*Sirpa* DC ii" clusters displayed a DC2-like profile being marked by expression of *Sirpa*, *Kmo, Cd209a* and Cd7 (**Fig. 4A & Supplementary Fig S7B**). The cells in these clusters also strongly expressed *PU.1*, but were distinguished by low *Flt3* expression suggesting that they may be moDC (*38, 45*) (**Fig 5**). The remaining two DC clusters comprised a set of *Xcr1*$^{high}$*Irf8*$^{high}$*Sirpa*$^{low}$ cells ("*Xcr1* DC") that are likely to correspond to conventional cDC1 cells and a small group of migratory *Ccr7* positive DCs ("*Ccr7* DC"). In comparison to that observed in uninfected animals, the MNP population structure at the peak of *Hh* + αIL10R induced inflammation (**Fig 4A,C**) showed a marked increase in the numbers of *Ly6c2*$^{hi}$*MhcII*$^{+}$ inflammatory monocytes, a larger and more heterogeneous DC population along with a diminished frequency of macrophages, consistent with above analysis (**Fig 2F and Supplementary Fig. S7C**).

When clusters were split by genotype, it was found that monocyte clusters had similar numbers of WT and *Irf5*$^{-/-}$ cells, whereas macrophage clusters, especially *Cd11c* Mϕ, had higher numbers of WT cells, while the *Sirpa* DC i and ii clusters contained higher numbers of *Irf5*$^{-/-}$ cells (**Fig. 4C**), findings which were confirmed by FACS-based analysis (**Supplementary Fig S7C**). The decrease in the frequency of *Irf5*$^{-/-}$ *Cd11c* Mϕ relative to WT was more striking during the peak of inflammation (**Fig 4C**) than at steady state (**Fig 3B**), suggesting that the propensity of IRF5 to promote generation of CD11c+ macrophages is accentuated by the inflammatory environment. Together with the fact that *CD11c*+ monocyte/macrophages can drive immunopathology(*9*) this observation provided a possible explanation for the pathogenic role of IRF5 in intestinal inflammation (**Fig. 2**).

**IRF5 defines an inflammatory MNP signature during colitis**

To investigate the effect of IRF5 on the transcriptional phenotype of intestinal monocytes and macrophages, we conducted small bulk RNA-seq analysis of WT and *Irf5*$^{-/-}$ Ly6C$^{hi}$MHCII$^{-}$ (P1) monocytes, Ly6C$^{hi}$MHCII$^{+}$ (P2) monocytes and Ly6C$^{-}$MHCII$^{+}$F4/80$^{+}$ macrophages (n=100 cells/sample) from each of the inflamed colons of three *Hh* + αIL10R mixed bone marrow chimera animals. First, we identified the genes that showed significant variation between the WT monocyte and macrophage samples. Hierarchical clustering of these genes revealed that the transcriptome of P2 monocytes overlaps with the profiles of both P1 monocytes and macrophages in line with the concept that they represent a transitional state of monocyte to macrophage differentiation (**Supplementary Fig. S8A**). We also detected high expression levels for genes previously shown to be associated with mature intestinal macrophages, such as MHC molecules (*H2-M2*), tetraspanins (*Cd72, Cd81*), complement molecules (*C1qa, C1qb, C1qc*), chemokines (*Ccl5, Ccl8*) and phagocytic and immunoactivating receptors (*Fcgr4, Fcer1g, Cd300e*) in the macrophage populations(*23*). Next, we identified genes that were significantly (BH adjusted $p < 0.05$, $|\text{fold change}| > 2$) regulated by IRF5 in each of the P1 (n=607 genes), P2 (n=761 genes) and macrophage (n=977 genes) compartments (**Supplementary Fig. S8B**). Amongst the differentially expressed genes, Ly6C$^{hi}$MHCII$^{-}$ *Irf5*$^{-/-}$ P1 monocytes showed significantly lower levels of *Smad2* and *Kdm3a* which respectively transduce and positively regulate TGF-B and Jak2/Stat3 signalling, pathways of known importance for monocyte maturation (**Fig. 5A**). In line with this observation IRF5 deficient macrophages failed to down-regulate genes highly expressed in P1 and P2 monocytes including *Plac8*,

*Cdkn2d* (*P19ink4d*) and *Irf1* and also showed significantly lower expression of the MHC class II molecule *H2-M2* (**Fig. 5A**). At the same time, in macrophages, loss of IRF5 reduced expression of the key pro-inflammatory cytokines (*Il-12b*, *Ccl11*, *Tnfsf13b/BAFF*), expression of the immunoactivating receptor *Cd300e*, tetraspanins (*Cd81* and *Cd72*) as well as *IL-10*. A significant reduction in the expression of the key pro-inflammatory cytokine *Il-12b* was also observed in the P2 monocytes. These changes were accompanied by up and down-regulation of the epigenetic regulators *Hdac2* and *Hdac9* in IRF5 deficient macrophages. At the pathway level, geneset enrichment analysis of Gene Ontology (GO) Biological Process categories revealed that IRF5 broadly modulated inflammatory pathways including “leukocyte activation”, “response to interferon-gamma”, “response to bacterium” and “regulation of T-cell activation” in both monocytes (P1 & P2), and macrophages (BH adjusted p-value < 0.1, **Fig. 5B**). Genes regulated by IRF5 in the P2 monocyte compartment displayed a significant enrichment of genes involved in “regulation of interleukin-12 production”, “interleukin 6-secretion”, “interleukin-1 production”, while genes associated with “response to interleukin-1” and “TNF superfamily cytokine production” were also affected in macrophages (**Fig. 5B**). These pathways, and specifically production of IL-23, IL-1, and TNF, have been previously associated with colitis development and/or IBD (*9, 29, 33*). In independent experiments, using flow cytometry, we confirmed that colonic WT macrophages in the MBMCs produced higher levels of cytokines TNFα and IL-1β cytokines than *Irf5*$^{-/-}$ cells (**Fig. 5C, D**). The surface expression of MHCII was higher on WT macrophages relative to *Irf5*$^{-/-}$ (**Fig. 5E**).

When small bulk RNA-seq data were compared to scRNA-Seq gene expression data, a good correspondence between the genes expressed in the *Ly6c* and *MHCII* monocyte clusters and P1 and P2 samples respectively was observed (**Supplementary Fig S8C**). Both the *Cd11c* and *Cd206* macrophage clusters showed similarities to the small-bulk macrophage sample (**Supplementary Fig S8C**).

**IRF5 promotes monocyte to *Cd11c* macrophage differentiation during intestinal inflammation**

Given the reduction in *Irf5*$^{-/-}$ macrophages numbers that we saw in the mixed bone marrow chimera at the peak of *Hh* + αIL10R induced colitis (**Fig 4C** and **Supplementary Fig S7C**) we examined an apparent role for IRF5 in controlling monocyte differentiation in more detail. First, we performed a global comparison of genes regulated by IRF5 in macrophages with those that were associated with differentiation from P1 monocytes to macrophages in the inflamed cLP. Overall, this analysis revealed a significant positive correlation between genes up-regulated during macrophage differentiation and those positively regulated by IRF5 in macrophages (Spearman's' rho: 0.45, $p = 5.5 \times 10^{-110}$) (**Supplementary Fig. S9**). Close examination of the scatter plot, however, also revealed a large number of genes that were up-regulated in macrophages independent of the presence of IRF5 including *C1qc*, *Ptgs1* (Cox1) and *Mmp13* (green dots, **Supplementary Fig. S9**). These data support a cell-intrinsic role for IRF5 in regulating myeloid cell differentiation and phenotype during intestinal inflammation.

To dissect the role of IRF5 in controlling MNP differentiation in the inflamed cLP in more detail we applied the Slingshot pseudo-time algorithm(*46*) to our scRNA-Seq data. After exclusion of the dendritic cells, higher-resolution analysis identified 6 clusters of monocytes and macrophages (**Supplementary Fig. S10**) that fell into three predicted lineages (with *Ly6c2* monocytes assumed to represent the 'root' state) (**Fig. 6A and 6B**). These represented the differentiation of (i) *Cd11c* (*Itgax*) macrophages that also expressed *Acp5*, (ii) *Cd206* (*Mrc1*) macrophages that were also positive for *Cd36*, *Ccl2* and *Ccl7* and (iii) a small population of *Clec4e* expressing mature ($MHCII^{hi}$) monocytes that resembled those found in the steady state data (see **Fig 3**). Most notably, the $Irf5^{-/-}$ cells were under-represented (4.3% vs 22% of WT cells) in the terminal cluster of the *Cd11c* lineage (**Fig 6C**, cluster 3) with progression of $Irf5^{-/-}$ cells in pseudotime along this lineage being significantly different to that of the wildtype cells (**Fig 6D**, Bonferroni adjusted $p = 2.2x10^{-6}$). The pseudotime distribution of $Irf5^{-/-}$ cells along the *Cd206* lineage was also significantly altered (Fig 6D, Bonferroni adjusted p=0.003) but this was associated with only a slight reduction in the number of $Irf5^{-/-}$ Cd206 macrophages (**Fig 6C**, cluster 4, 8.5% vs 11.7% of WT cells). In contrast, a similar percentage of $Irf5^{-/-}$ and WT cells were found in the *Clec4e* monocyte cluster (**Fig 6C**, cluster 5) and there was no difference between the progression of $Irf5^{-/-}$ and WT cells along this lineage (**Fig 6D**).

The reduction of $Irf5^{-/-}$ cells in the macrophage clusters was paralleled by an increase in the number of $Irf5^{-/-}$ cells in the immature Ly6c2 monocyte cluster (cluster 2, 23.0% vs 14.6% WT cells) and differentiating monocyte cluster (cluster 0, 36% vs 20.6% of WT cells) (**Fig 6C**). These data suggest that IRF5 may promote the acquisition of CD11c expression by $Ly6C^{hi}MHCII^{+}$ monocytes and their differentiation to $CD11c^{+}$ macrophages.

**CD11c$^+$ macrophages occupy a distinct colonic niche**

We assessed the localisation of CD206+ and CD11c+ macrophage subsets in the colon, by performing labelling of colonic tissue sections with antibodies against CD11c, CD206 and F4/80 and subsequent analysis by confocal microscopy (**Fig 7A**). This analysis revealed that the two macrophage subsets localized at distinct sites at steady state. CD206+/F4/80+ cells (CD206+ macrophages) dominated the colonic macrophage pool and were located within the lamina propria, with some found to be residing at the base of intestinal crypts (**Fig 7B**). Macrophages at the base of crypts are believed to be involved in response to the mucosal barrier damage via secretion of CCL8 (*42*) and other chemokines and may transmit regenerative signals to neighbouring colonic epithelial progenitors (*47*). Indeed, chemokines (*Ccl2, Ccl7, Cxcl2*) were distinctively expressed in C*d206* Mϕs during *Hh* + αIL10R-induced colitis (**Supplementary Fig S11A**).

CD11c+ F4/80+ cells (CD11c+ macrophages) were more sparsely located and mainly found at the luminal surface (**Fig 7B**). Thus, CD11c$^+$ macrophages may represent a primed macrophage phenotype, ready to respond to microbial encroachment (*21*). In fact, many genes specifically expressed in C*d11c* Mϕs during *Hh* + αIL10R-induced colitis belonged to an anti-microbial defence programme (*Dnase1l3, Acp5, Mmp14 etc*) and protein recycling (*Ctsa, Ctsh, Ctsz*) (**Supplementary Fig S11A**). We quantified the distance of the macrophage subsets in relation to the luminal surface and the serosal membrane (**Fig 7C**). At steady state, CD11c+ macrophages were found to be significantly closer to the luminal surface than CD206+ macrophages, but this proximity was lost

during inflammation (**Fig 7D**), when CD206+ and CD11c+ macrophages started to intersperse throughout the cLP and at the muscularis mucosae membrane (**Fig 7B**).

**IRF5 controls the phenotype of CD11c$^+$ macrophages**

Previously, CD11c$^+$F4/80$^+$ monocytes and macrophages were shown to be critical effector cells in the development of *Hh* + αIL10R-induced experimental colitis via the production of IL-23 (*9*). Here we confirmed that CD11c$^+$F4/80$^+$ macrophages (**Supplementary Fig. S11B**) produced higher levels of IL-12p40, a subunit of IL-23 (**Fig. 8A**), as well as other inflammatory cytokines, such as TNF and IL-1β, than CD11c$^-$ macrophages (**Fig. 8B,C**). In the setting of the mixed bone marrow chimera, we confirmed that IRF5 promoted the development of CD11c$^+$ macrophages both at the peak of *Hh* + αIL10R induced colitis (**Fig. 8D**) and in steady state (**Supplementary Fig. S11C**). In keeping with this observation, the expression of IRF5 protein was higher in CD11c$^+$ macrophages and Ly6C$^{hi}$MHCII$^+$ monocytes, compared to their CD11c$^-$ counterparts (**Fig 8E and Supplementary Fig 11D**).

At the peak of *Hh* + αIL10R induced colitis IRF5 positively regulated a cassette of genes that defined cLP macrophage phenotypes, such as MHC molecules (*H2-M2*), tetraspanins (*Cd72, Cd81*), complement molecules (*C1q*), chemokines (*Ccl4*), acid phosphatase 5 (*Acp5*) and phagocytic and immunoactivating receptors (*Fcgr4, Fcer1g, Cd300e*) in the *Cd11c* Mϕ population. A number of killer cell lectin-like receptor family members (*Klrb1b, Klra2, Klra17*), not previously associated with macrophage function were also affected by the lack of IRF5 in this compartment (**Fig 8F**). Together our data

show that IRF5 promotes the differentiation and inflammatory phenotype of Cd11c+ macrophages during *Hh* + αIL10R induced colitis.

## Discussion

Using a model of mononuclear phagocyte development in the gut and a combination of mixed bone marrow chimera approaches and single cell analysis of gene expression, we have demonstrated the importance of IRF5 in promoting the generation of macrophages in the cLP. We found that it dictates an inflammatory $CD11c^{+}F4/80^{+}$ macrophage phenotype in inflammation, and controls the immunopathology of *Hh* + αIL10R-induced colitis.

Our results revealed a cell-intrinsic role for IRF5 in the control of a wide-range of genes and biological pathways related to monocyte differentiation, leukocyte activation, response to bacterium, pattern recognition receptor signalling pathway and regulation of T-cell activation in inflamed intestine (**Fig 5**). Indeed, mice with a global or MNP-specific loss of IRF5 were protected from *Hh* + αIL10R colitis (**Fig. 2**). In comparison, IRF5 had a much more limited impact on gene expression at steady state intestine (**Figs 1,3**) and we observed no morphological differences in cLP between WT and *Irf5*$^{-/-}$ at steady state (**Fig 1**), consistent with the recently published report (*48*).

The most consistent function of IRF5 identified in this study is its ability to promote a pro-inflammatory monocyte and macrophage state, which is positive for CD11c. Cd11c+ macrophages were found at the luminal surface at homeostasis and throughout the cLP in inflammation (**Fig 7**). They transcribe anti-microbial molecules, such as cathepsins, and are efficient producers of inflammatory cytokines, such as TNF and IL-1β, that support pathogenic T cell responses in the intestine(*34, 49, 50*) (**Fig 8 and Supplementary Fig S8**). $CD11c^{+}$ macrophages produce high quantities of IL-23 in the

early stages of Helicobacter hepaticus induced colitis and are essential for triggering intestinal immunopathology (*9, 15*). They are also essential producers of IL-1b and IL-23 in Citrobacter rodentium induced colitis (*21*). CD11c+ intestinal macrophages were marked by high level of IRF5 (**Fig. 8**). IRF5 deficiency ameliorated the accumulation of $CD11c^+$ macrophages in cLP (**Fig. 8D, Supplementary Fig S11B**). With the recently established link between $CD11c^+$ macrophages and IRF5 in the development of atherosclerotic lesions (*51*), our data here support the notion that IRF5 may guide monocyte differentiation towards inflammatory $CD11c^+$ macrophages in a variety of tissues and pathologies. While we only found a subtle effect for IRF5 on monocyte development in the bone marrow and subset conversion in the blood at steady state (**Supplementary Fig S4**), it is possible that it has a larger effect in these compartments during inflammation.

The second major population of macrophages detected in our analyses was marked by the expression of CD206 and predominantly located at the base of crypts at steady state (**Fig. 7**). These macrophages expressed phagocytic receptors, the scavenger receptor *Cd36*, which is critical for lysosomal lipolysis (*52*), the anti-inflammatory gene *Ifitm3* (*41*), *Alox5ap* involved in leukotriene biosynthetic pathway, and a milieu of chemokines (Ccl2, Ccl7, Cxcl2 etc) (**Figs 3, 4 and Supplementary Fig. S11**). These may represent resident macrophages involved in the clearance of senescent epithelial and apoptotic cells, sensing and regulating response to mucosal damage and possibly contributing to epithelial renewal. The *Cd206* macrophages appeared largely unaffected by IRF5 deficiency (**Fig. 3**) and unlikely to be major contributors to the *Hh*-induced pathology(*33*). Pseudo-time analysis of our scRNA-seq data indicate that the *Cd206* and *Cd11*c

macrophages broadly represent alternative macrophage differentiation trajectories during intestinal inflammation (**Fig. 6**). Together with the distinct distribution of these two macrophage populations in the cLP (**Fig. 7**) and their unequal dependence on IRF5 (**Fig. 8**) these data suggest that they may emerge independently in specific environmental niches. In fact, our steady state single-cell data (**Fig 3**) suggest that there is substantial heterogeneity within both the *Cd206* and *Cd11c* macrophage populations (the Cd206 populations can be readily split, for example, by Cd14 status) and further imaging and lineage tracing studies are needed to resolve the niches, origins and functions of these subsets. In both our steady state and inflamed single cell datasets we noted the presence of a small mature (*MHCII*$^{hi}$), activated (*Rel*$^{+ve}$, *Nlrp3*$^{+ve}$) *Clec4e*$^{hi}$ monocyte (*F4/80*$^{-ve}$) population that appeared unaffected by absence of IRF5 (**Fig. 3** and **Fig. 6**). Given the known roles of Clec4e (Mincle), a C-type lectin receptor (CLR), these cells may play important roles in host defence and tissue repair in the intestine (*53*).

The *Cd206* macrophages in the cLP transcribed high levels of CCL2 (**Fig. 4**), a critical chemokine for accumulation of monocytes in the cLP (*20*). Consistent with previously published analysis (*39*), we observed more efficient recruitment of donor WT than donor *Irf5*$^{-/-}$ monocytes to cLP in the mixed bone marrow chimera animals, highlighting another mechanism by which IRF5 could modulate inflammation *i.e*. via controlling a pathogenic positive-feedback loop of inflammatory monocyte recruitment.

Finally, our data suggest that in an inflammatory environment, IRF5 specifically promotes key aspects of macrophage differentiation whilst repressing DC transition (**Fig. 4**). The observed changes in expression of the histone deacetylases *Hdac2* and *Hdac9* **(Fig 5)** may be consistent with a role for IRF5 in controlling of the epigenetic state of these cells.

This process may be due to loss of competition for IRF binding sites, and engagement of an IRF4-dependent differentiation program(*54, 55*). IRF4 and IRF5 were shown to compete for binding to Myeloid Differentiation primary response 88 (MyD88) and activation following TLR4 ligation(*56*). IRF4 is a key regulator of intestinal CD11b$^{+}$ DC subsets and a critical transcription factor in the DC fate of monocytes in *in vitro* bone marrow cultures(*55, 57*). Thus, in the absence of IRF5, IRF4 may be able to dominate the fate choice of monocytes, explaining the increased predisposition to DC fate in *Irf5*$^{-/-}$.

Although intestinal DCs are believed to be largely derived of FLT3L-dependent progenitors (*13*), several studies have provided evidence that *Sirpa* CD11b$^{+}$ DCs are replenished by monocytes in the inflamed cLP (*16, 17*). It is intriguing that *MHCII+Cd209+* blood monocytes, previously identified as precursors of moDCs (*38*), showed the highest number of genes affected by the lack of IRF5, while all other monocyte populations remained largely unaffected **(Supplementary Fig S4, S6A)**. This may reflect the more advanced differentiated state of *MHCII+Cd209+* monocytes, but more functional characterisation of the populations are needed.

In summary, the data presented here reveals that IRF5 controls the MNP system in the colon, is a critical driver of intestinal inflammation and promotes monocyte differentiation towards bactericidal and inflammatory CD11c+ macrophages.

## Materials and Methods

### Study Design

The purpose of this study was to understand the intrinsic role of IRF5 in directing macrophage polarisation and intestinal inflammation. Flow cytometry, bulk- and single cell-RNA-sequencing, and immunofluorescence labelling of intestinal tissue sections were used to analyse the leukocyte milieu in the colons of wild type or *Irf5*$^{-/-}$ or mixed bone marrow chimeric mice. Mice were aged between 8-16 weeks at the commencement of experiments. Experimental sample sizes were not predetermined. *Helicobacter hepaticus* infections were ended upon mouse sacrifice at d21 post-infection. In general, experiments were performed at least twice unless indicated otherwise. Data were not excluded from analysis except for QC failures in RNAseq analysis detailed in **Material and Methods (Supplementary materials)**. Histopathology assessment was conducted in a blinded manner independently by two researchers. Experimenters were not blinded to intervention groups for flow cytometry analysis.

### Data availability

Next generation sequencing datasets are available via the Gene Expression Omnibus (GEO) via accession codes GSE129354 (GM-DMDM data) and GSE129258 (MBMC small bulk and single-cell data).

## SUPPLEMENTARY MATERIALS

## References


1. K. J. Maloy, F. Powrie, Intestinal homeostasis and its breakdown in inflammatory bowel disease. *Nature* **474**, 298 (2011).
2. R. V. Bryant, O. Brain, S. P. L. Travis, Conventional drug therapy for inflammatory bowel disease. *Scandinavian Journal of Gastroenterology* **50**, 90-112 (2015).
3. I. Bravatà, G. Fiorino, M. Allocca, A. Repici, S. Danese, New targeted therapies such as anti-adhesion molecules, anti-IL-12/23 and anti-Janus kinases are looking toward a more effective treatment of inflammatory bowel disease. *Scandinavian Journal of Gastroenterology* **50**, 113-120 (2015).
4. G. Meuret, A. Bitzi, B. Hammer, Macrophage turnover in Crohn's disease and ulcerative colitis. *Gastroenterology* **74**, 501-503 (1978).
5. A. J. Bune, A. R. Hayman, M. J. Evans, T. M. Cox, Mice lacking tartrate-resistant acid phosphatase (Acp 5) have disordered macrophage inflammatory responses and reduced clearance of the pathogen, Staphylococcus aureus. *Immunology* **102**, 103-113 (2001).
6. J. H. Niess, S. Brand, X. Gu, L. Landsman, S. Jung, B. A. McCormick, J. M. Vyas, M. Boes, H. L. Ploegh, J. G. Fox, D. R. Littman, H.-C. Reinecker, CX3CR1-Mediated Dendritic Cell Access to the Intestinal Lumen and Bacterial Clearance. *Science* **307**, 254-258 (2005).
7. O. Schulz, E. Jaensson, E. K. Persson, X. Liu, T. Worbs, W. W. Agace, O. Pabst, Intestinal CD103(+), but not CX3CR1(+), antigen sampling cells migrate in lymph and serve classical dendritic cell functions. *The Journal of Experimental Medicine* **206**, 3101-3114 (2009).
8. J. Cosin-Roger, D. Ortiz-Masia, S. Calatayud, C. Hernandez, J. V. Esplugues, M. D. Barrachina, The activation of Wnt signaling by a STAT6-dependent macrophage phenotype promotes mucosal repair in murine IBD. *Mucosal Immunol* **9**, 986-998 (2016).
9. I. C. Arnold, S. Mathisen, J. Schulthess, C. Danne, A. N. Hegazy, F. Powrie, CD11c+ monocyte/macrophages promote chronic Helicobacter hepaticus-induced intestinal inflammation through the production of IL-23. *Mucosal Immunol* **9**, 352-363 (2016).
10. M. H. Jang, N. Sougawa, T. Tanaka, T. Hirata, T. Hiroi, K. Tohya, Z. Guo, E. Umemoto, Y. Ebisuno, B.-G. Yang, J.-Y. Seoh, M. Lipp, H. Kiyono, M. Miyasaka, CCR7 Is Critically Important for Migration of Dendritic Cells in Intestinal Lamina Propria to Mesenteric Lymph Nodes. *The Journal of Immunology* **176**, 803 (2006).
11. J. J. Worthington, B. I. Czajkowska, A. C. Melton, M. A. Travis, Intestinal Dendritic Cells Specialize to Activate Transforming Growth Factor-β and Induce Foxp3(+) Regulatory T Cells via Integrin αvβ8. *Gastroenterology* **141**, 1802-1812 (2011).
12. C. C. Bain, J. Montgomery, C. L. Scott, J. M. Kel, M. J. H. Girard-Madoux, L. Martens, T. F. P. Zangerle-Murray, J. Ober-Blöbaum, D. Lindenbergh-Kortleve, J. N. Samsom, S. Henri, T. Lawrence, Y. Saeys, B. Malissen, M. Dalod, B. E. Clausen, A. M. Mowat, TGFβR signalling controls CD103+CD11b+ dendritic cell development in the intestine. *Nature Communications* **8**, 620 (2017).
13. T. Joeris, K. Muller-Luda, W. W. Agace, A. M. Mowat, Diversity and functions of intestinal mononuclear phagocytes. *Mucosal Immunol* **10**, 845-864 (2017).

14. J. Sheng, Q. Chen, I. Soncin, S. L. Ng, K. Karjalainen, C. Ruedl, A Discrete Subset of Monocyte-Derived Cells among Typical Conventional Type 2 Dendritic Cells Can Efficiently Cross-Present. *Cell Reports* **21**, 1203-1214 (2017).
15. E. Zigmond, C. Varol, J. Farache, E. Elmaliah, Ansuman T. Satpathy, G. Friedlander, M. Mack, N. Shpigel, Ivo G. Boneca, Kenneth M. Murphy, G. Shakhar, Z. Halpern, S. Jung, Ly6Chi Monocytes in the Inflamed Colon Give Rise to Proinflammatory Effector Cells and Migratory Antigen-Presenting Cells. *Immunity* **37**, 1076-1090 (2012).
16. A. Rivollier, J. He, A. Kole, V. Valatas, B. L. Kelsall, Inflammation switches the differentiation program of Ly6Chi monocytes from antiinflammatory macrophages to inflammatory dendritic cells in the colon. *The Journal of Experimental Medicine* **209**, 139 (2012).
17. H. A. Schreiber, J. Loschko, R. A. Karssemeijer, A. Escolano, M. M. Meredith, D. Mucida, P. Guermonprez, M. C. Nussenzweig, Intestinal monocytes and macrophages are required for T cell polarization in response to Citrobacter rodentium. *The Journal of Experimental Medicine* **210**, 2025-2039 (2013).
18. T. N. Shaw, S. A. Houston, K. Wemyss, H. M. Bridgeman, T. A. Barbera, T. Zangerle-Murray, P. Strangward, A. J. L. Ridley, P. Wang, S. Tamoutounour, J. E. Allen, J. E. Konkel, J. R. Grainger, Tissue-resident macrophages in the intestine are long lived and defined by Tim-4 and CD4 expression. *The Journal of Experimental Medicine*, (2018).
19. C. C. Bain, A. Bravo-Blas, C. L. Scott, E. Gomez Perdiguero, F. Geissmann, S. Henri, B. Malissen, L. C. Osborne, D. Artis, A. M. Mowat, Constant replenishment from circulating monocytes maintains the macrophage pool in the intestine of adult mice. *Nat Immunol* **15**, 929-937 (2014).
20. C. C. Bain, C. L. Scott, H. Uronen-Hansson, S. Gudjonsson, O. Jansson, O. Grip, M. Guilliams, B. Malissen, W. W. Agace, A. M. Mowat, Resident and pro-inflammatory macrophages in the colon represent alternative context-dependent fates of the same Ly6Chi monocyte precursors. *Mucosal Immunol* **6**, 498-510 (2013).
21. S.-U. Seo, P. Kuffa, S. Kitamoto, H. Nagao-Kitamoto, J. Rousseau, Y.-G. Kim, G. Núñez, N. Kamada, Intestinal macrophages arising from CCR2+ monocytes control pathogen infection by activating innate lymphoid cells. *Nature Communications* **6**, 8010 (2015).
22. A. Bujko, N. Atlasy, O. J. B. Landsverk, L. Richter, S. Yaqub, R. Horneland, O. Øyen, E. M. Aandahl, L. Aabakken, H. G. Stunnenberg, E. S. Bækkevold, F. L. Jahnsen, Transcriptional and functional profiling defines human small intestinal macrophage subsets. *The Journal of Experimental Medicine* **215**, 441 (2018).
23. A. Schridde, C. C. Bain, J. U. Mayer, J. Montgomery, E. Pollet, B. Denecke, S. W. F. Milling, S. J. Jenkins, M. Dalod, S. Henri, B. Malissen, O. Pabst, A. McL Mowat, Tissue-specific differentiation of colonic macrophages requires TGF[beta] receptor-mediated signaling. *Mucosal Immunol*, (2017).
24. E. Zigmond, B. Bernshtein, G. Friedlander, Catherine R. Walker, S. Yona, K.-W. Kim, O. Brenner, R. Krauthgamer, C. Varol, W. Müller, S. Jung, Macrophage-Restricted Interleukin-10 Receptor Deficiency, but Not IL-10 Deficiency, Causes Severe Spontaneous Colitis. *Immunity* **40**, 720-733 (2014).

25. T. Krausgruber, K. Blazek, T. Smallie, S. Alzabin, H. Lockstone, N. Sahgal, T. Hussell, M. Feldmann, I. A. Udalova, IRF5 promotes inflammatory macrophage polarization and TH1-TH17 responses. *Nat Immunol* **12**, 231-238 (2011).
26. A. Balasa, G. Gathungu, P. Kisfali, E. O. B. Smith, J. H. Cho, B. Melegh, R. Kellermayer, Assessment of DNA methylation at the interferon regulatory factor 5 (IRF5) promoter region in inflammatory bowel diseases. *International Journal of Colorectal Disease* **25**, 553-556 (2010).
27. V. Dideberg, G. Kristjansdottir, L. Milani, C. Libioulle, S. Sigurdsson, E. Louis, A.-C. Wiman, S. Vermeire, P. Rutgeerts, J. Belaiche, D. Franchimont, A. Van Gossum, V. Bours, A.-C. Syvänen, An insertion–deletion polymorphism in the Interferon Regulatory Factor 5 (IRF5) gene confers risk of inflammatory bowel diseases. *Human Molecular Genetics* **16**, 3008-3016 (2007).
28. G. Gathungu, C. K. Zhang, W. Zhang, J. H. Cho, A two-marker haplotype in the IRF5 gene is associated with inflammatory bowel disease in a North American cohort. *Genes And Immunity* **13**, 351 (2012).
29. M. F. Neurath, Cytokines in inflammatory bowel disease. *Nat Rev Immunol* **14**, 329-342 (2014).
30. M. C. Kullberg, D. Jankovic, C. G. Feng, S. Hue, P. L. Gorelick, B. S. McKenzie, D. J. Cua, F. Powrie, A. W. Cheever, K. J. Maloy, A. Sher, IL-23 plays a key role in Helicobacter hepaticus–induced T cell–dependent colitis. *The Journal of Experimental Medicine* **203**, 2485-2494 (2006).
31. M. C. Kullberg, J. M. Ward, P. L. Gorelick, P. Caspar, S. Hieny, A. Cheever, D. Jankovic, A. Sher, Helicobacter hepaticus Triggers Colitis in Specific-Pathogen-Free Interleukin-10 (IL-10)-Deficient Mice through an IL-12- and Gamma Interferon-Dependent Mechanism. *Infection and Immunity* **66**, 5157-5166 (1998).
32. M. C. Kullberg, D. Jankovic, P. L. Gorelick, P. Caspar, J. J. Letterio, A. W. Cheever, A. Sher, Bacteria-triggered CD4(+) T Regulatory Cells Suppress Helicobacter hepaticus–induced Colitis. *The Journal of Experimental Medicine* **196**, 505-515 (2002).
33. C. C. Bain, C. J. Oliphant, C. A. Thomson, M. C. Kullberg, A. M. Mowat, Proinflammatory Role of Monocyte-Derived CX3CR1$^{int}$ Macrophages in *Helicobacter hepaticus*-Induced Colitis. *Infection and Immunity* **86**, (2018).
34. P. P. Ahern, A. Izcue, K. J. Maloy, F. Powrie, The interleukin-23 axis in intestinal inflammation. *Immunological Reviews* **226**, 147-159 (2008).
35. J. Farache, I. Koren, I. Milo, I. Gurevich, K.-W. Kim, E. Zigmond, G. C. Furtado, S. A. Lira, G. Shakhar, Luminal Bacteria Recruit CD103(+) Dendritic Cells into the Intestinal Epithelium to Sample Bacterial Antigens for Presentation. *Immunity* **38**, 581-595 (2013).
36. A. Mortha, A. Chudnovskiy, D. Hashimoto, M. Bogunovic, S. P. Spencer, Y. Belkaid, M. Merad, Microbiota-Dependent Crosstalk Between Macrophages and ILC3 Promotes Intestinal Homeostasis. *Science* **343**, (2014).
37. A. Mildner, J. Schönheit, A. Giladi, E. David, D. Lara-Astiaso, E. Lorenzo-Vivas, F. Paul, L. Chappell-Maor, J. Priller, A. Leutz, I. Amit, S. Jung, Genomic Characterization of Murine Monocytes Reveals C/EBP[beta]; Transcription Factor Dependence of Ly6C$^{-}$ Cells. *Immunity* **46**, 849-862.e847 (2017).

38. S. Menezes, D. Melandri, G. Anselmi, T. Perchet, J. Loschko, J. Dubrot, R. Patel, E. L. Gautier, S. Hugues, M. P. Longhi, J. Y. Henry, S. A. Quezada, G. Lauvau, A.-M. Lennon-Duménil, E. Gutiérrez-Martínez, A. Bessis, E. Gomez-Perdiguero, C. E. Jacome-Galarza, H. Garner, F. Geissmann, R. Golub, M. C. Nussenzweig, P. Guermonprez, The Heterogeneity of Ly6Chi Monocytes Controls Their Differentiation into iNOS+ Macrophages or Monocyte-Derived Dendritic Cells. *Immunity* **45**, 1205-1218 (2016).
39. L. Yang, D. Feng, X. Bi, R. C. Stone, B. J. Barnes, Monocytes from Irf5(−/−) mice have an intrinsic defect in their response to pristane-induced lupus. *Journal of immunology (Baltimore, Md. : 1950)* **189**, 3741-3750 (2012).
40. G. A. Leung, T. Cool, C. H. Valencia, A. Worthington, A. E. Beaudin, E. C. Forsberg, The lymphoid-associated interleukin 7 receptor (IL7R) regulates tissue-resident macrophage development. *Development* **146**, (2019).
41. Z. Alteber, A. Sharbi-Yunger, M. Pevsner-Fischer, D. Blat, L. Roitman, E. Tzehoval, E. Elinav, L. Eisenbach, The anti-inflammatory IFITM genes ameliorate colitis and partially protect from tumorigenesis by changing immunity and microbiota. *Immunol Cell Biol* **96**, 284-297 (2018).
42. K. Asano, N. Takahashi, M. Ushiki, M. Monya, F. Aihara, E. Kuboki, S. Moriyama, M. Iida, H. Kitamura, C. H. Qiu, T. Watanabe, M. Tanaka, Intestinal CD169(+) macrophages initiate mucosal inflammation by secreting CCL8 that recruits inflammatory monocytes. *Nat Commun* **6**, 7802 (2015).
43. P. Jha, H. Das, KLF2 in Regulation of NF-kappaB-Mediated Immune Cell Function and Inflammation. *Int J Mol Sci* **18**, (2017).
44. D. A. Anderson, G. E. Grajales-Reyes, A. T. Satpathy, C. E. Vasquez Hueichucura, T. L. Murphy, K. M. Murphy, Revisiting the specificity of the MHC class II transactivator CIITA in classical murine dendritic cells in vivo. *European Journal of Immunology* **47**, 1317-1323 (2017).
45. L. Richter, O. J. B. Landsverk, N. Atlasy, A. Bujko, S. Yaqub, R. Horneland, O. Øyen, E. M. Aandahl, K. E. A. Lundin, H. G. Stunnenberg, E. S. Bækkevold, F. L. Jahnsen, Transcriptional profiling reveals monocyte-related macrophages phenotypically resembling DC in human intestine. *Mucosal Immunology* **11**, 1512-1523 (2018).
46. K. Street, D. Risso, R. B. Fletcher, D. Das, J. Ngai, N. Yosef, E. Purdom, S. Dudoit, Slingshot: cell lineage and pseudotime inference for single-cell transcriptomics. *BMC Genomics* **19**, 477 (2018).
47. S. L. Pull, J. M. Doherty, J. C. Mills, J. I. Gordon, T. S. Stappenbeck, Activated macrophages are an adaptive element of the colonic epithelial progenitor niche necessary for regenerative responses to injury. *Proc Natl Acad Sci U S A* **102**, 99-104 (2005).
48. S. P. Pandey, J. Yan, J. R. Turner, C. Abraham, Reducing IRF5 expression attenuates colitis in mice, but impairs the clearance of intestinal pathogens. *Mucosal Immunol* **12**, 874-887 (2019).
49. K. Ghoreschi, A. Laurence, X.-P. Yang, C. M. Tato, M. J. McGeachy, J. Konkel, H. L. Ramos, L. Wei, T. Davidson, N. Bouladoux, J. Grainger, Q. Chen, Y. Kanno, W. T. Watford, H.-W. Sun, G. Eberl, E. Shevach, Y. Belkaid, D. J. Cua, W. Chen, J. J.

O'Shea, Generation of Pathogenic Th17 Cells in the Absence of TGF-β Signaling. *Nature* **467**, 967-971 (2010).
50. M. Coccia, O. J. Harrison, C. Schiering, M. J. Asquith, B. Becher, F. Powrie, K. J. Maloy, IL-1β mediates chronic intestinal inflammation by promoting the accumulation of IL-17A secreting innate lymphoid cells and CD4+ Th17 cells. *The Journal of Experimental Medicine* **209**, 1595 (2012).
51. A. N. Seneviratne, A. O. Edsfeldt, J. E. Cole, C. Kassiteridi, M. Swart, I. Park, P. Green, T. E. Khoyratty, D. G. Saliba, M. E. Goddard, S. N. Sansom, I. Goncalves, R. Krams, I. A. Udalova, C. Monaco, Interferon Regulatory Factor 5 Controls Necrotic Core Formation in Atherosclerotic Lesions by Impairing Efferocytosis. *Circulation*, (2017).
52. S. C. Huang, B. Everts, Y. Ivanova, D. O'Sullivan, M. Nascimento, A. M. Smith, W. Beatty, L. Love-Gregory, W. Y. Lam, C. M. O'Neill, C. Yan, H. Du, N. A. Abumrad, J. F. Urban, Jr., M. N. Artyomov, E. L. Pearce, E. J. Pearce, Cell-intrinsic lysosomal lipolysis is essential for alternative activation of macrophages. *Nat Immunol* **15**, 846-855 (2014).
53. X. Lu, M. Nagata, S. Yamasaki, Mincle: 20 years of a versatile sensor of insults. *Int Immunol* **30**, 233-239 (2018).
54. D. Xu, F. Meyer, E. Ehlers, L. Blasnitz, L. Zhang, Interferon Regulatory Factor 4 (IRF-4) Targets IRF-5 to Regulate Epstein-Barr Virus Transformation. *Journal of Biological Chemistry* **286**, 18261-18267 (2011).
55. C. Goudot, A. Coillard, A.-C. Villani, P. Gueguen, A. Cros, S. Sarkizova, T.-L. Tang-Huau, M. Bohec, S. Baulande, N. Hacohen, S. Amigorena, E. Segura, Aryl Hydrocarbon Receptor Controls Monocyte Differentiation into Dendritic Cells versus Macrophages. *Immunity* **47**, 582-596.e586 (2017).
56. H. Negishi, Y. Ohba, H. Yanai, A. Takaoka, K. Honma, K. Yui, T. Matsuyama, T. Taniguchi, K. Honda, Negative regulation of Toll-like-receptor signaling by IRF-4. *Proceedings of the National Academy of Sciences of the United States of America* **102**, 15989-15994 (2005).
57. Emma K. Persson, H. Uronen-Hansson, M. Semmrich, A. Rivollier, K. Hägerbrand, J. Marsal, S. Gudjonsson, U. Håkansson, B. Reizis, K. Kotarsky, William W. Agace, IRF4 Transcription-Factor-Dependent CD103+CD11b+ Dendritic Cells Drive Mucosal T Helper 17 Cell Differentiation. *Immunity* **38**, 958-969 (2013).
58. A. Butler, P. Hoffman, P. Smibert, E. Papalexi, R. Satija, Integrating single-cell transcriptomic data across different conditions, technologies, and species. *Nature Biotechnology* **36**, 411 (2018).

## Figure legends

### Figure 1: IRF5 deficiency has limited impact on colon physiology at steady-state

**A)** Representative H&E sections of colons from WT (left) and *Irf5*$^{-/-}$ (right) mice at steady state. **B)** Histopathology scoring of WT (n=6) and *Irf5*$^{-/-}$ (n=5) colons. **C)** Number of cLPLs retrieved from steady state WT (n=9) and *Irf5*$^{-/-}$ (n=5) mice. **D)** IRF5 expression in the steady state cLP of WT mice (n=3). **E)** The frequency of intestinal MNPs in the cLP of steady state WT (n=9) and *Irf5*$^{-/-}$ (n=5) mice. **F)** Quantification of early phase (Annexin V$^{+}$ Live/Dead$^{-}$), and late phase (Annexin V$^{+}$ Live/Dead$^{+}$) cell death assessed by Annexin V labelling combined with viability dye staining in WT (n=3) and *Irf5*$^{-/-}$ (n=3) cLP Ly6C$^{hi}$ MHC II$^{+}$ (P2) monocytes and macrophages using flow cytometry immediately after cell isolation. **B, C, E:** Data are pooled from two independent experiments. **D, F:** data are representative of two independent experiments. **B, C)** Mann-Whitney U test. **E, F)** Two-Way ANOVA with Sidak correction. Data presented are mean ± SEM, ns = not significant, ** $p \leq 0.01$

### Figure 2: IRF5 deficiency protects against intestinal inflammation

**A)** Representative H&E sections of colons from WT (left) and *Irf5*$^{-/-}$ (right) mice at d21 *Hh* + αIL10R. **B)** Histopathology scoring of WT and *Irf5*$^{-/-}$ colons. **C)** Number of cLPLs retrieved from steady state and d21 *Hh* + αIL10R WT and *Irf5*$^{-/-}$ mice. **D)** frequencies of IFNγ-, IL17A- and IFNγ/IL17-producing CD4$^{+}$ T cells in WT and *Irf5*$^{-/-}$ mice following 4 hours of culture with PMA/Ionomycin and brefeldin assessed by intracellular flow cytometry. **E)** Spleen weights of WT and *Irf5*$^{-/-}$ mice at steady state and d21 *Hh* + αIL10R. **B,E:** Data are representative of two independent experiments, (ss n=3, *Hh* + αIL10R n=7).

Two-Way ANOVA with Tukey correction. **C,D:** Data are representative of two independent experiments, (WT ss n=6, *Irf5*$^{-/-}$ ss n = *3 Hh* + αIL10R n=7). Two-Way ANOVA with Tukey correction. **F)** The frequency of intestinal MNPs in the cLP at d21 *Hh* + αIL10R WT (n=12) and *Irf5*$^{-/-}$ (n=11) mice. **G)** Representative H&E sections of colons from $CX_3CR1^{IRF5+}$ (left) and $CX_3CR1^{IRF5-}$ (right) mice at d21 *Hh* + αIL10R. **H)** Histopathology scoring of colons from $CX_3CR1^{IRF5+}$ (n=11) and $CX_3CR1^{IRF5-}$ (n=11) mice at d21 *Hh* + αIL10R.. **F,H:** Data are pooled from two independent experiments. **F)** Two-Way ANOVA with Sidak correction, **H)** Unpaired t-test. Data presented are mean ± SEM, ns = not significant, * $p \leq 0.05$, ** $p \leq 0.01$, *** $p \leq 0.001$, **** $p < 0.0001$

**Figure 3: IRF5 has subtle effect on CD11c+ intestinal macrophages at steady state**

WT and *Irf5*$^{-/-}$ $CD45^+CD11b^+SiglecF^-Ly6G^-CX_3CR1^+$ cells were sorted from the colons of five mixed bone marrow chimera animals and subjected to scRNA-Seq analysis. **A)** Graph based clustering(*58*) of equal numbers of WT and *Irf5*$^{-/-}$ cells (n=4780 total) identified nine clusters of MNPs and one cluster of dendritic cells. **B)** The bar plots show the percentages of WT and *Irf5*$^{-/-}$ cells that were found in each cluster. Panels **C)** – **F)** show the expression of cell type markers **C)**, genes expressed in *Cd11c*$^{+ve}$ macrophages **D)**, genes expressed in *Mrc1*$^{+ve}$ macrophages and genes with associated with macrophage differentiation and activation **E)**.

**Figure 4: IRF5 promotes generation of CD11c+ macrophages in inflamed colon**

WT and *Irf5*$^{-/-}$ $CD45^+CD11b^+SiglecF^-Ly6G^-CX_3CR1^+$ cells were sorted from the colons of three mixed bone marrow chimera animals at d21 of *Hh* + αIL10R colitis and subjected to droplet-based single cell transcriptomic analysis. **A)** Graph based clustering(*58*) of

equal numbers of WT and *Irf5*$^{-/-}$ cells (n=1106 total) identified four clusters of MNPs and four clusters of dendritic cells. **B)** The violin plots show the expression levels (x axes) of selected known cLP MNP and DC sub-population markers in each of the identified clusters (y axes). **C)** The bar plots show the percentages of WT and *Irf5*$^{-/-}$ cells that were found in each cluster.

**Figure 5: IRF5 defines an inflammatory MNP signature during colitis**

WT and *Irf5*$^{-/-}$ P1 monocytes, P2 monocytes and macrophages were sorted from three mixed bone marrow chimera animals at d21 *Hh* + αIL10R. **A)** The dot plot shows the expression (mean TPM, n=3 biological replicates) of selected genes found to be differentially expressed between WT and Irf5$^{-/-}$ cells at one or more stages of the monocyte waterfall. The significant changes ($|fc| > 2$, BH adjusted $p < 0.05$) are indicated by the grey triangles. **B)** Selected GO Biological process categories that showed a significant enrichment (coloured dots, GSEA analysis, BH adjusted $p < 0.1$) in at least one of the three Irf5 KO vs WT small bulk RNA-seq comparisons. **C-E)** Intracellular or extracellular flow cytometry labelling was used to quantify the expression of **C)** TNFα, **D)** pro-IL1β, **E)** MHC II on WT vs *Irf5*$^{-/-}$ macrophages in mixed bone marrow chimera uninfected (n=3), and at d21 *Hh* + αIL10R colitis (n=4). Two-Way ANOVA with Sidak Correction. Data from one representative experiment presented are mean ± SEM, ns = not significant, * $p \leq 0.05$, ** $p \leq 0.01$, *** $p \leq 0.001$

**Figure 6: IRF5 promotes monocyte to Cd11c macrophage differentiation during intestinal inflammation** WT and Irf5$^{-/-}$ monocytes and macrophages from the inflamed intestine (**Fig 4**) were re-clustered at higher resolution (**Supplementary Fig S10**) and subject to pseudotime analysis. **A)** Embedding of the cells in the first three dimensions of

a diffusion map shows the three differentiation trajectories (solid lines) identified by the Slingshot pseudotime algorithm (with the *Ly6c2* monocytes assumed to represent the root state) **B)** Expression of selected cell type marker genes and genes associated with *Cd11c* (*Itgax*) an *Mrc1* (Cd206) macrophages. **C)** The bar plots show the percentages of WT and *Irf5*$^{-/-}$ cells that were found in each cluster. **D)** The violin plots show the progression of the WT and Irf5$^{-/-}$ (KO) cells through pseudotime along the three identified trajectories (as shown in **A)**). Differences in the distribution of cells in pseudotime between the genotypes were assessed with a KS tests (p-values adjusted using the Bonferroni correction). The position of the cells in pseudotime is shown on top of the violin plots (cells colored by cluster as in **A)**). The position of the 50$^{th}$ quantiles is indicated by the bold vertical lines.

**Figure 7: CD11c+ macrophages occupy a distinct colonic niche**

**A**) Representative images of immunofluorescent labelling of colonic sections at steady state. Individual channels visualise the distribution of F4/80+ (blue), CD206+ (green) and CD11c+ (red) cells within the structure of the colon. CD206+ macrophages (white arrow) and CD11c+ macrophages (*) as well as single-positive F4/80+ cells (#) can be detected in the merged image. Cell nuclei are labelled with Sytoxblue (grey). Scalebars represent 50 µM. **B**) Localisation of double-positive CD11c+F4/80+ (cyan) and CD206+F4/80 (yellow) cells, in steady state (n=6) and colitic mouse colons (n=6) by immunehistofluorescence. Separate channels based on overlap of staining were created. Cell nuclei were labelled with Sytoxblue (grey). A minimum of 5 sections per mouse were evaluated. Macrophages at the base of the crypts (white arrow), at the tips of the villi (*), interspersed within the villi (†); at the Muscularis mucosae membrane (#). Scalebars represent 100 µM in the overview images and 50µM in the enlargement. **C**) Schematic

depiction of image quantification analysis. Localisation of macrophages is assessed by their minimal distance (black arrow) to the tip of the villi (artificial luminal surface depicted in green), muscularis mycosae (red) and serosal membranes (blue). **D**) Quantification of minimal distance of CD206+ F4/80+ and CD11c+ F4/80+ cells in steady state and d21 *Hh* + αIL10R to the luminal surface. Minimal distance is presented as a percentage of the distance to the tip of the villi to the total distance between the luminal surface and serosal membrane. Two-way Anova with Tukey's multiple comparisons test. Data presented as mean ± SEM, ns $p > 0.05$, * $p < 0.05$, ** $p < 0.01$, *** $p < 0.001$.

**Figure 8: IRF5 controls phenotype of CD11c+ macrophages**

**A, B, C)** Comparison of IL12p40, TNF and IL-1β inflammatory cytokine expression in $CD11c^+$ vs $CD11c^-$ cLP macrophages assessed by intracellular flow cytometry, in uninfected MBMC (n=3) and d21 *Hh* + αIL10R (n=4). One experiment. Two-Way ANOVA with Tukey Correction. Data presented are mean ± SEM, ns = not significant, * $p \leq 0.05$, **** $p < 0.0001$. **D)** The frequency of parent WT and *Irf5*$^{-/-}$ macrophages expressing CD11c or CD206 at d21 *Hh* + αIL10R colitis. Two-Way ANOVA with Sidak Correction. Data presented are mean ± SEM from two independent experiments, ns = not significant, **** $p < 0.0001$. **E)** IRF5 expression in $CD11c^+$ vs $CD11c^-$ macrophages in mixed bone marrow chimera assessed by intracellular flow cytometry. One representative experiment, uninfected n=3, *Hh* + αIL10R n=4. **F)** Heatmap of expression of selected genes in WT and *Irf5*$^{-/-}$ *Cd11c* macrophages from the inflamed cLP of the mixed bone marrow chimeras (see **Fig 5**). All of the genes shown were found to be significantly differentially expressed between the WT and *Irf5*$^{-/-}$ cells of this cluster (Wilcoxon tests, BH adjusted $p < 0.05$). *'s

denote significant differential expression between the genotypes in the macrophage small-bulk RNA-seq data.

## Acknowledgements:

We are grateful to S. Teichmann (Wellcome Sanger Institute) for help in establishing Smart-Seq2 protocol and generating preliminary data that inspired our subsequent single cell analysis. We thank the High-Throughput Genomics Group (Wellcome Trust Centre for Human Genetics) for the generation of the sequencing data; C. Pearson for assistance with the generation of mixed bone marrow chimaeras; J. Webber for assistance with cell sorting, and the Kennedy Institute Histopathology Team for sectioning and staining of mouse colons.

**Funding:**

This work was supported by the Kennedy Trust for Rheumatology Research (ALC, MGV, DB, SNS), the MRC CGAT programme (SNS), the Novo Nordisk Foundation (Tripartite Immunometabolism Consortium - grant NNF15CC0018486 to IAU), and the Wellcome Trust (Investigator Award 095688/Z/11/Z to FP and 209422/Z/17/Z to IAU).

**Author contributions:**

ALC performed all experiments, except as noted below; MGV and SNS performed all computational analyses; DLB conducted immunofluorescence microscopy; MA generated scRNA-seq libraries; ICA provided advice and assisted with H.h infections and phenotype analysis; IAU, SNS and FP devised and directed the study. ALC, IAU, SNS wrote the manuscript.

**Competing financial interests:**

FP received research funding or consultancy fees from GSK, Genentech, Roche and UCB. Other authors declare that they have no competing interests.

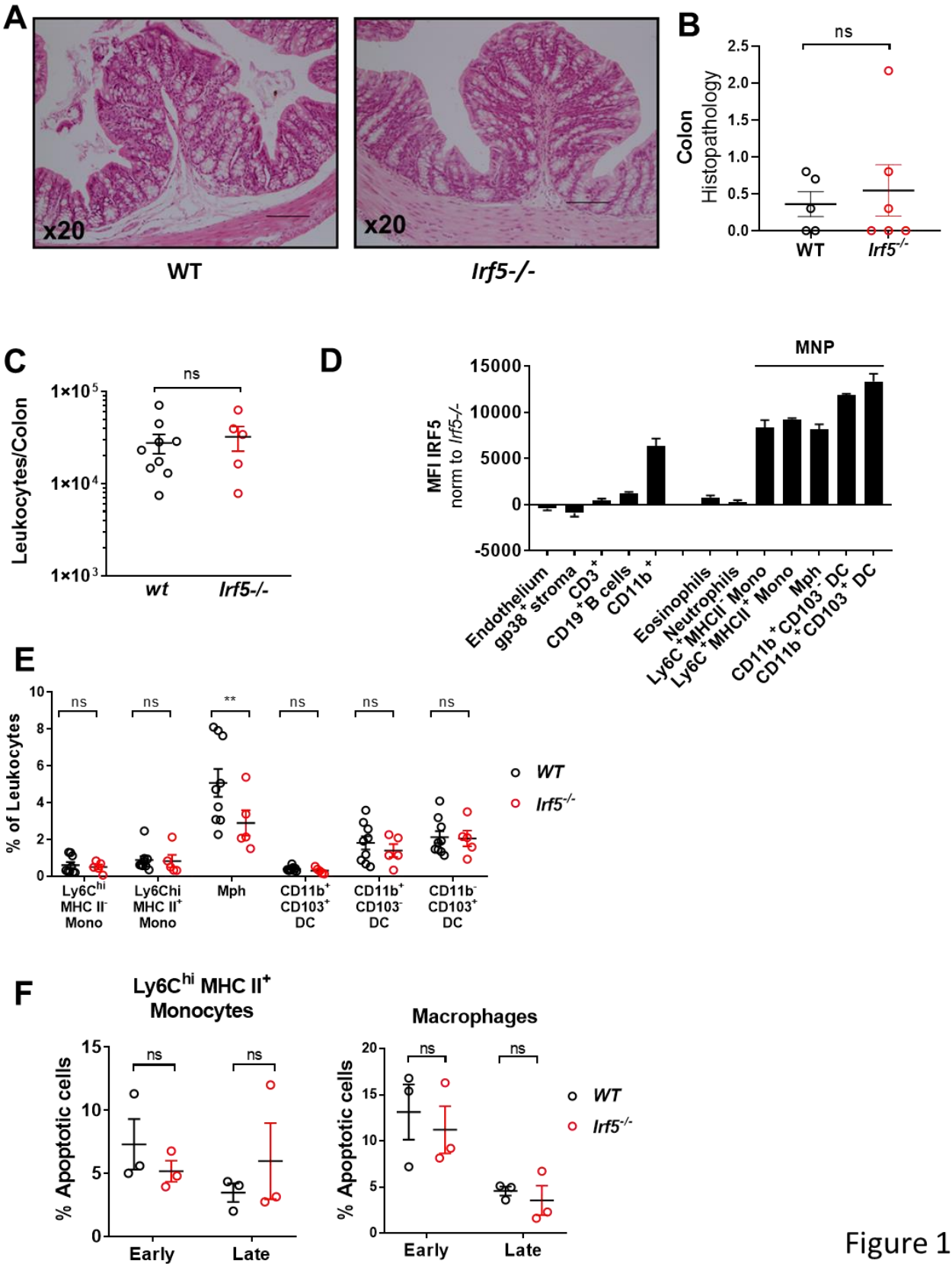
A
x20
x20
WT
Irf5-/-
B
ns
Colon Histopathology
2.5
2.0
1.5
1.0
0.5
0.0
WT
Irf5-/-
C
ns
Leukocytes/Colon
1×10^5
1×10^4
1×10^3
wt
Irf5-/-
D
MNP
MFI IRF5 norm to Irf5-/-
15000
10000
5000
0
-5000
Endothelium
gp38+ stroma
CD3+
CD19+ B cells
CD11b+
Eosinophils
Neutrophils
Ly6C+MHCII- Mono
Ly6C+MHCII+ Mono
Mph
CD11b+CD103- DC
CD11b+CD103+ DC
E
% of Leukocytes
10
8
6
4
2
0
ns
ns
**
ns
ns
ns
Ly6Chi MHC II- Mono
Ly6Chi MHC II+ Mono
Mph
CD11b+ CD103+ DC
CD11b+ CD103- DC
CD11b- CD103+ DC
WT
Irf5-/-
F
Ly6Chi MHC II+ Monocytes
Macrophages
% Apoptotic cells
15
10
5
0
20
ns
ns
ns
ns
Early
Late
Early
Late
WT
Irf5-/-

Figure 1

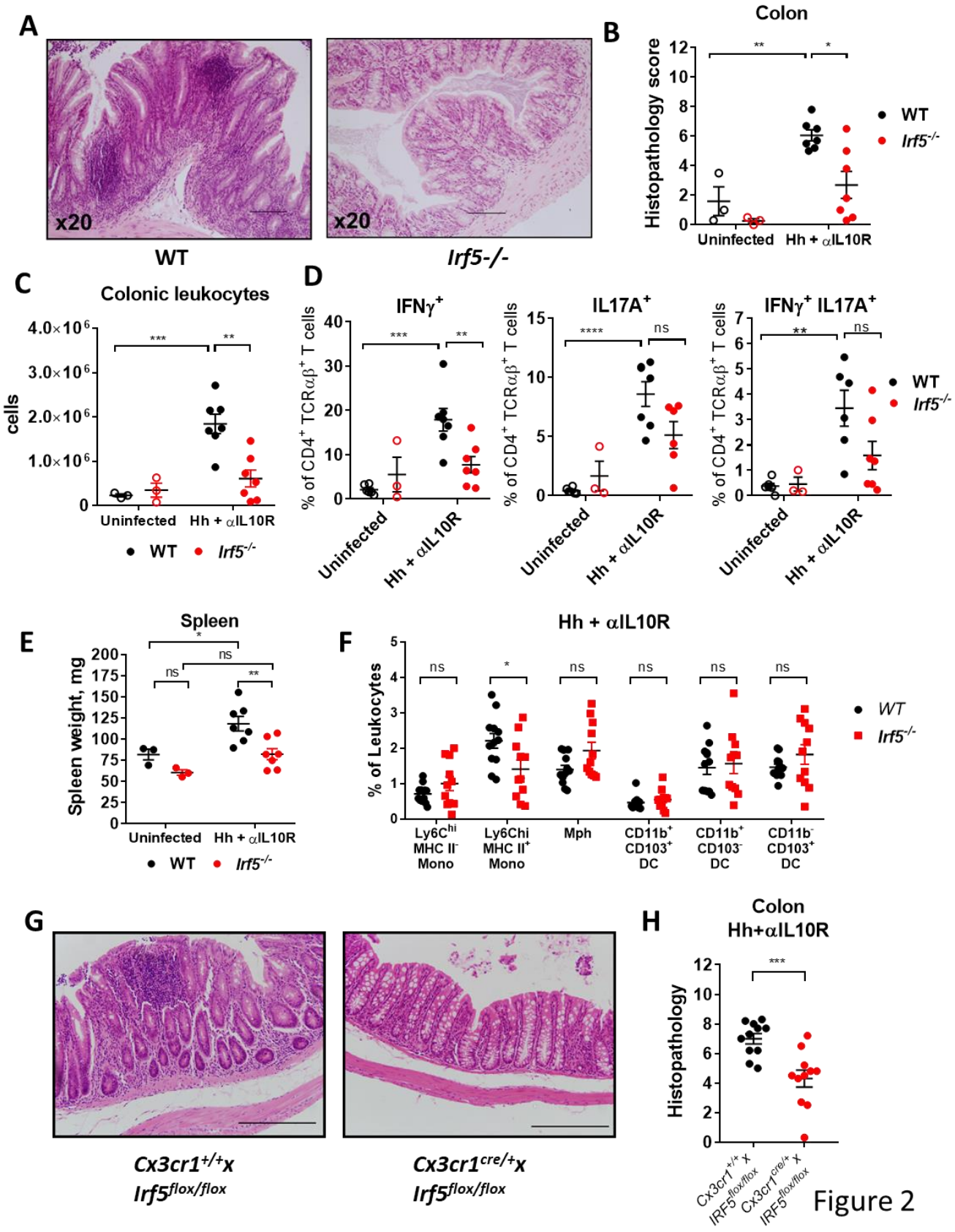
A
x20
x20
WT
Irf5-/-
B
Colon
Histopathology score
WT
Irf5-/-
Uninfected
Hh + αIL10R
C
Colonic leukocytes
cells
WT
Irf5-/-
D
IFNγ+
IL17A+
IFNγ+ IL17A+
% of CD4+ TCRαβ+ T cells
E
Spleen
Spleen weight, mg
F
Hh + αIL10R
% of Leukocytes
Ly6Chi MHC II- Mono
Ly6Chi MHC II+ Mono
Mph
CD11b+ CD103+ DC
CD11b+ CD103- DC
CD11b- CD103+ DC
G
Cx3cr1+/+x Irf5flox/flox
Cx3cr1cre/+x Irf5flox/flox
H
Colon Hh+αIL10R
Histopathology

Figure 2

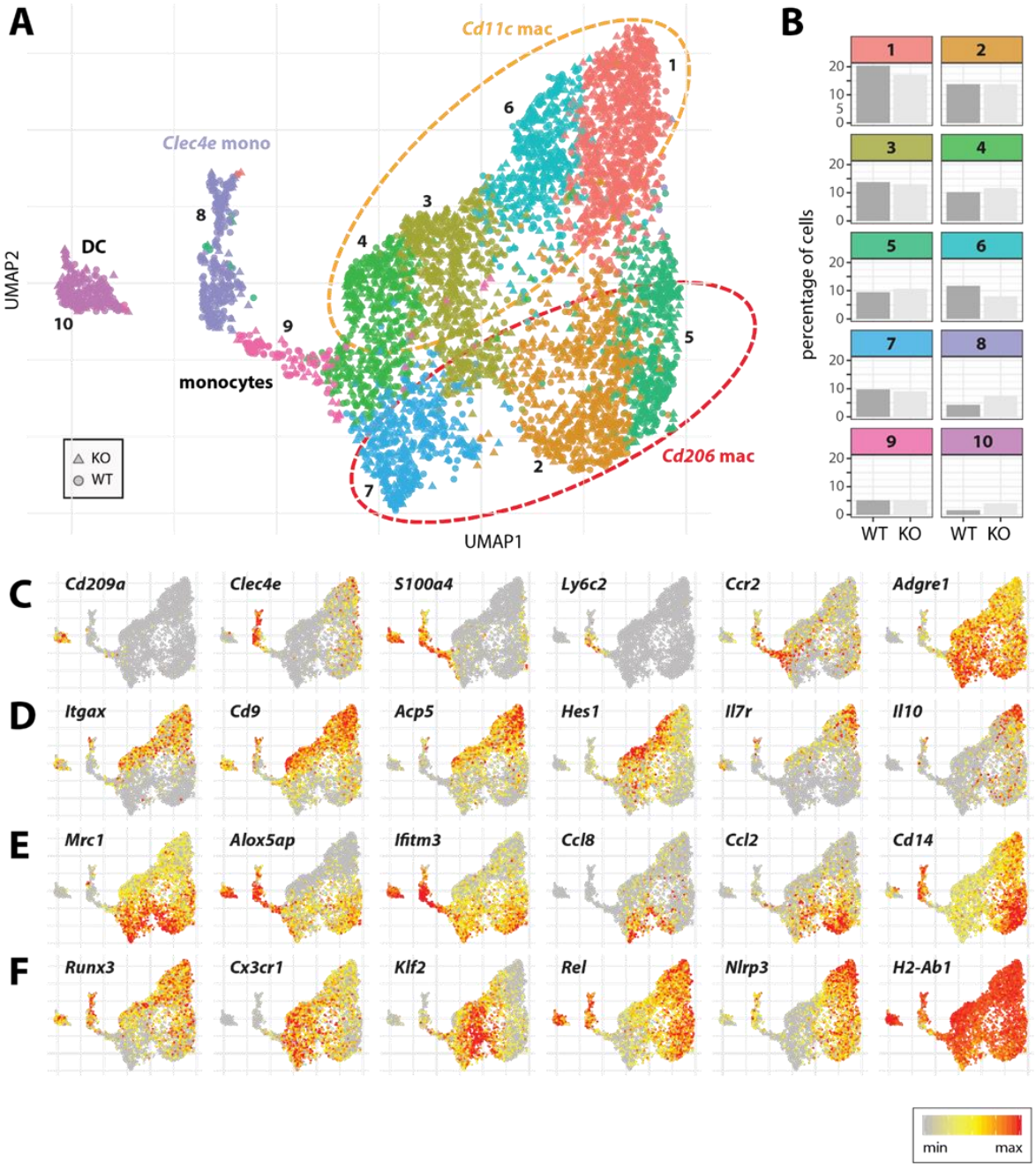
A
Cd11c mac
Clec4e mono
DC
monocytes
Cd206 mac
UMAP1
UMAP2
KO
WT
B
percentage of cells
WT KO WT KO
C
Cd209a
Clec4e
S100a4
Ly6c2
Ccr2
Adgre1
D
Itgax
Cd9
Acp5
Hes1
Il7r
Il10
E
Mrc1
Alox5ap
Ifitm3
Ccl8
Ccl2
Cd14
F
Runx3
Cx3cr1
Klf2
Rel
Nlrp3
H2-Ab1
min
max

Figure 3

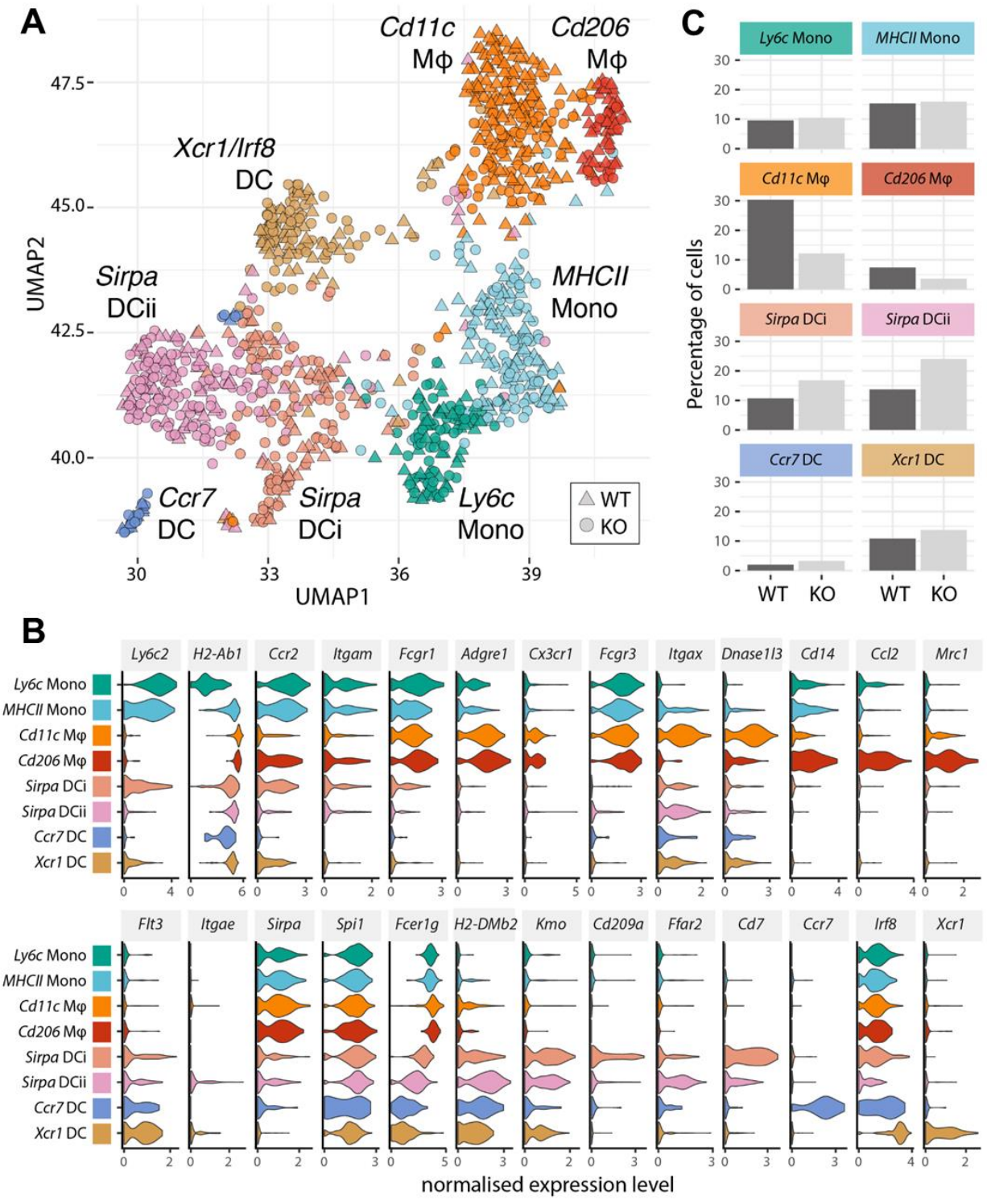
A
Cd11c Mϕ
Cd206 Mϕ
Xcr1/Irf8 DC
Sirpa DCii
MHCII Mono
Ccr7 DC
Sirpa DCi
Ly6c Mono
WT
KO
UMAP1
UMAP2
C
Ly6c Mono
MHCII Mono
Cd11c Mϕ
Cd206 Mϕ
Sirpa DCi
Sirpa DCii
Ccr7 DC
Xcr1 DC
Percentage of cells
B
Ly6c2
H2-Ab1
Ccr2
Itgam
Fcgr1
Adgre1
Cx3cr1
Fcgr3
Itgax
Dnase1l3
Cd14
Ccl2
Mrc1
Flt3
Itgae
Sirpa
Spi1
Fcer1g
H2-DMb2
Kmo
Cd209a
Ffar2
Cd7
Ccr7
Irf8
Xcr1
normalised expression level

Figure 4

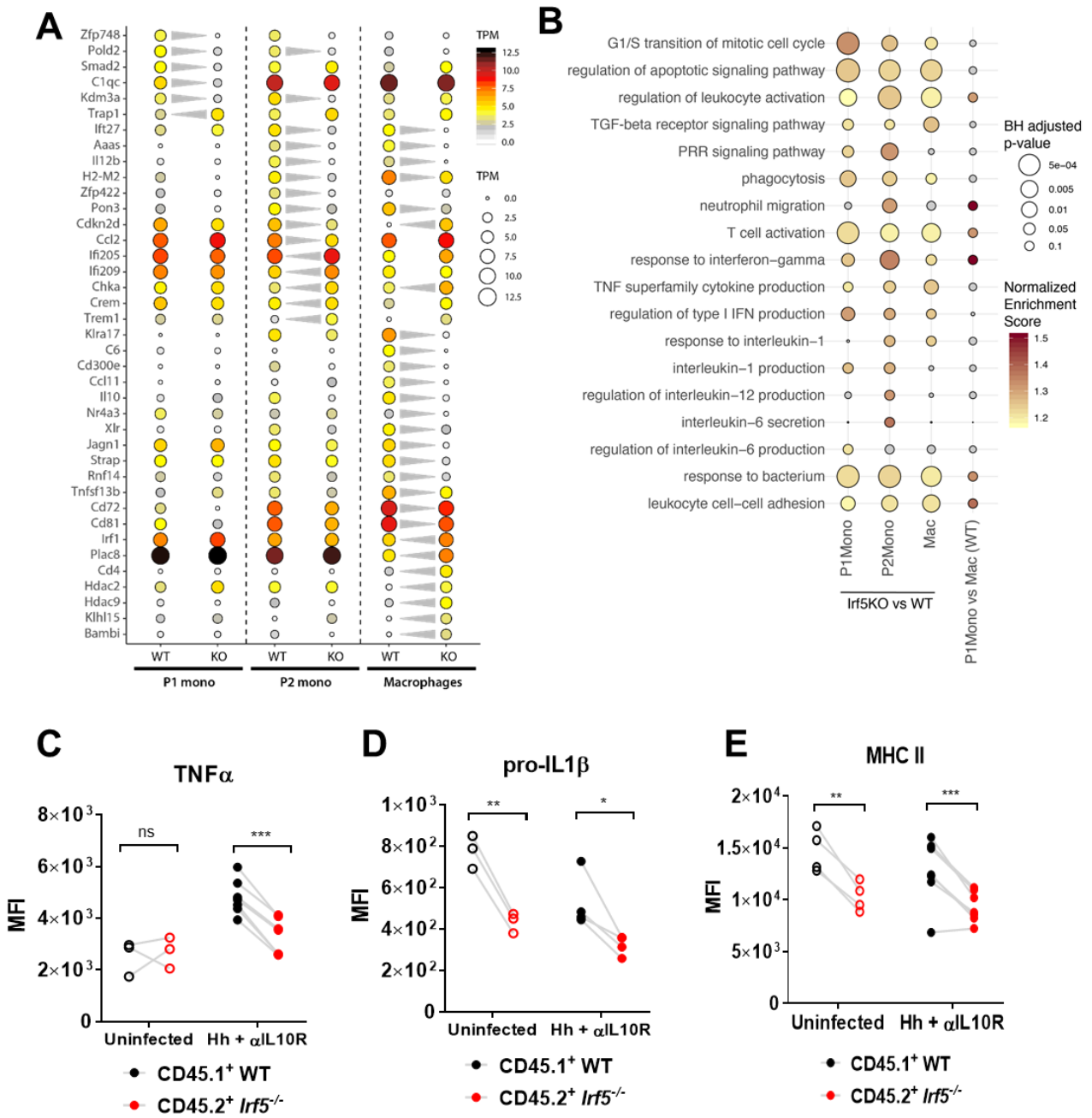
A
Zfp748
Pold2
Smad2
C1qc
Kdm3a
Trap1
Ift27
Aaas
Il12b
H2-M2
Zfp422
Pon3
Cdkn2d
Ccl2
Ifi205
Ifi209
Chka
Crem
Trem1
Klra17
C6
Cd300e
Ccl11
Il10
Nr4a3
Xlr
Jagn1
Strap
Rnf14
Tnfsf13b
Cd72
Cd81
Irf1
Plac8
Cd4
Hdac2
Hdac9
Klhl15
Bambi
TPM
12.5
10.0
7.5
5.0
2.5
0.0
WT
KO
P1 mono
P2 mono
Macrophages
B
G1/S transition of mitotic cell cycle
regulation of apoptotic signaling pathway
regulation of leukocyte activation
TGF-beta receptor signaling pathway
PRR signaling pathway
phagocytosis
neutrophil migration
T cell activation
response to interferon–gamma
TNF superfamily cytokine production
regulation of type I IFN production
response to interleukin–1
interleukin–1 production
regulation of interleukin–12 production
interleukin–6 secretion
regulation of interleukin–6 production
response to bacterium
leukocyte cell–cell adhesion
P1Mono
P2Mono
Mac
Irf5KO vs WT
P1Mono vs Mac (WT)
BH adjusted p-value
5e–04
0.005
0.01
0.05
0.1
Normalized Enrichment Score
1.5
1.4
1.3
1.2
C
TNFα
MFI
ns
***
Uninfected
Hh + αIL10R
CD45.1+ WT
CD45.2+ Irf5-/-
D
pro-IL1β
**
*
E
MHC II
**
***

Figure 5

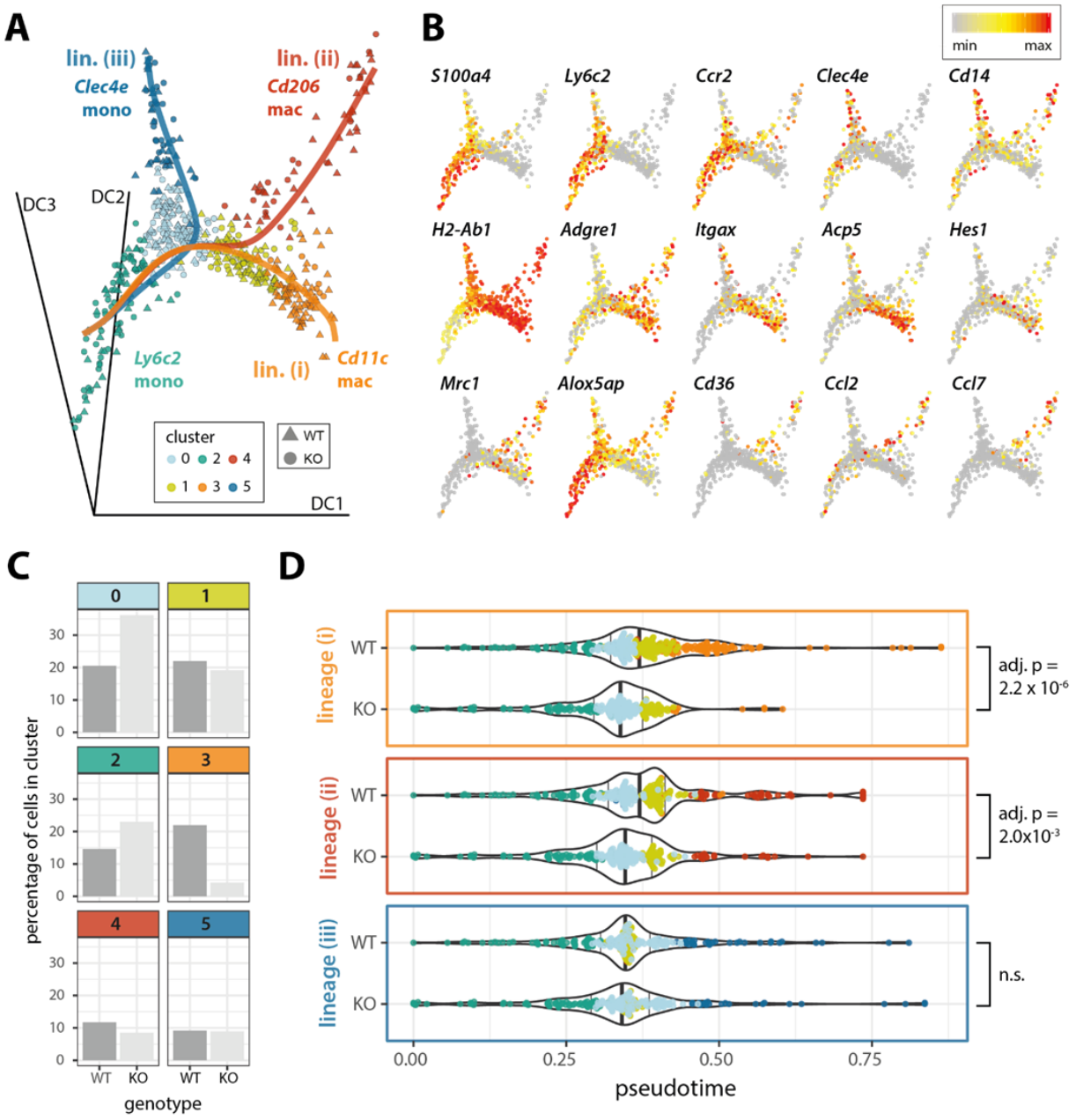
A
lin. (iii)
Clec4e
mono
lin. (ii)
Cd206
mac
DC3
DC2
Ly6c2
mono
lin. (i)
Cd11c
mac
cluster
0 2 4
1 3 5
WT
KO
DC1
B
min
max
S100a4
Ly6c2
Ccr2
Clec4e
Cd14
H2-Ab1
Adgre1
Itgax
Acp5
Hes1
Mrc1
Alox5ap
Cd36
Ccl2
Ccl7
C
percentage of cells in cluster
genotype
WT
KO
D
lineage (i)
lineage (ii)
lineage (iii)
adj. p = 2.2 x 10-6
adj. p = 2.0x10-3
n.s.
pseudotime

Figure 6

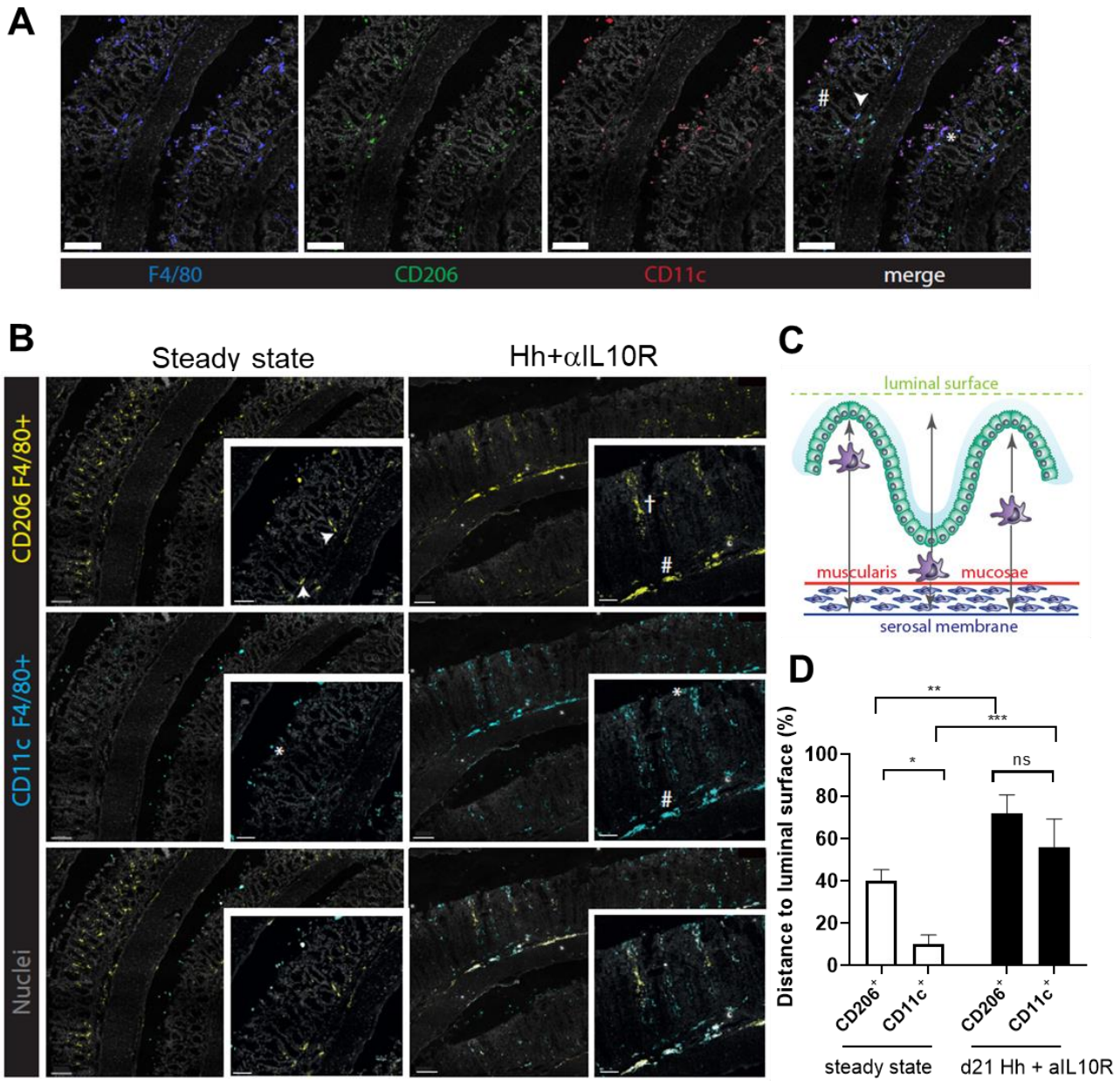
A
F4/80
CD206
CD11c
merge
B
Steady state
Hh+αIL10R
CD206 F4/80+
CD11c F4/80+
Nuclei
C
luminal surface
muscularis
mucosae
serosal membrane
D
Distance to luminal surface (%)
100
80
60
40
20
0
**
***
*
ns
CD206+
CD11c+
CD206+
CD11c+
steady state
d21 Hh + aIL10R

Figure 7

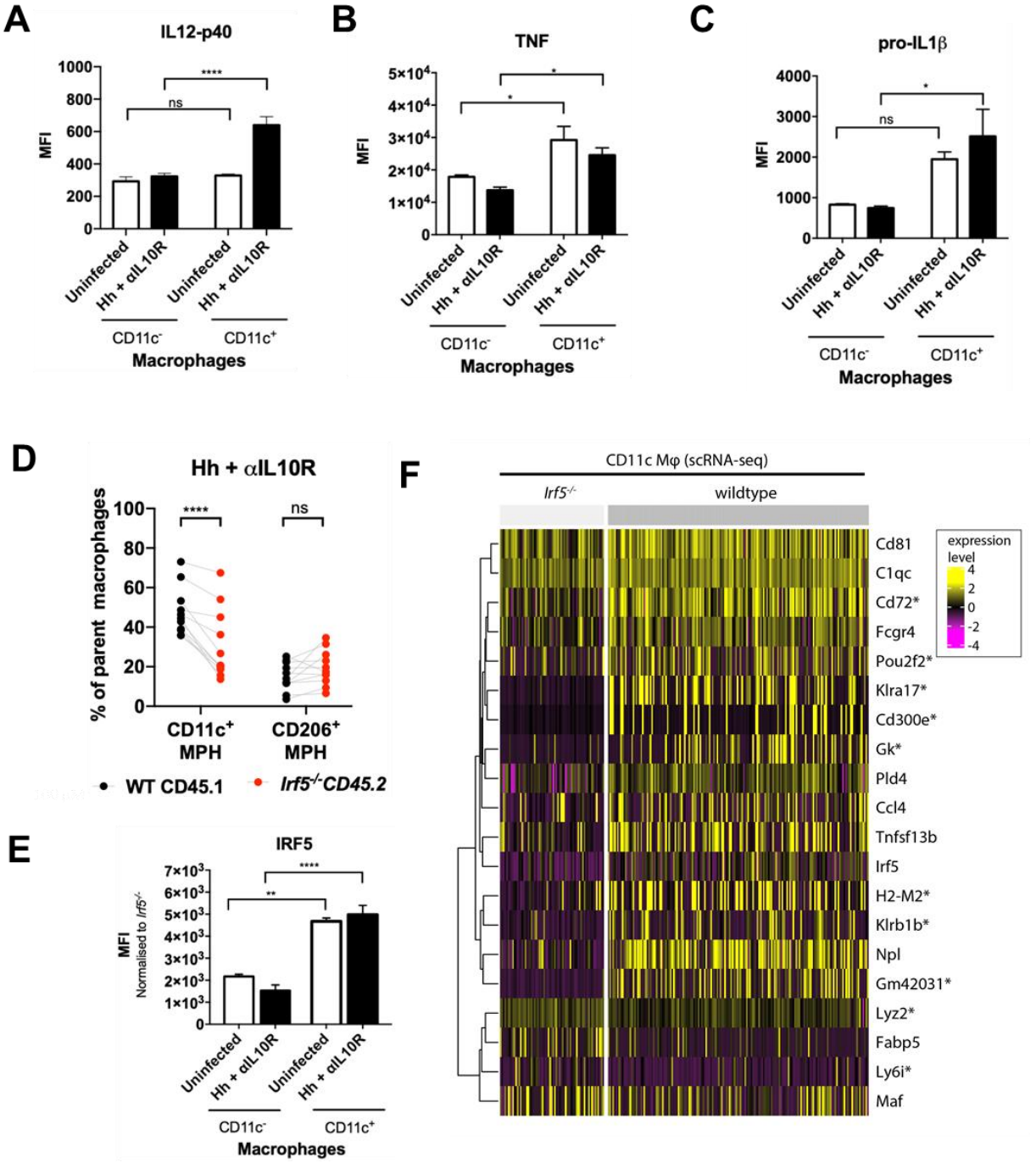
A
IL12-p40
MFI
1000
800
600
400
200
0
****
ns
Uninfected
Hh + αIL10R
Uninfected
Hh + αIL10R
CD11c-
CD11c+
Macrophages
B
TNF
MFI
5×10^4
4×10^4
3×10^4
2×10^4
1×10^4
0
*
*
Uninfected
Hh + αIL10R
Uninfected
Hh + αIL10R
CD11c-
CD11c+
Macrophages
C
pro-IL1β
MFI
4000
3000
2000
1000
0
*
ns
Uninfected
Hh + αIL10R
Uninfected
Hh + αIL10R
CD11c-
CD11c+
Macrophages
D
Hh + αIL10R
% of parent macrophages
100
80
60
40
20
0
****
ns
CD11c+ MPH
CD206+ MPH
WT CD45.1
Irf5-/-CD45.2
E
IRF5
MFI
Normalised to Irf5-/-
7×10^3
6×10^3
5×10^3
4×10^3
3×10^3
2×10^3
1×10^3
0
****
**
Uninfected
Hh + αIL10R
Uninfected
Hh + αIL10R
CD11c-
CD11c+
Macrophages
F
CD11c Mφ (scRNA-seq)
Irf5-/-
wildtype
expression level
4
2
0
-2
-4
Cd81
C1qc
Cd72*
Fcgr4
Pou2f2*
Klra17*
Cd300e*
Gk*
Pld4
Ccl4
Tnfsf13b
Irf5
H2-M2*
Klrb1b*
Npl
Gm42031*
Lyz2*
Fabp5
Ly6i*
Maf

Figure 8

## SUPPLEMENTARY MATERIALS

## Materials and Methods

### Animals

Mice were bred and maintained under SPF conditions in accredited animal facilities at the University of Oxford. All procedures were conducted according to the Operations of Animals in Scientific Procedures Act (ASPA) of 1986 and approved by the Kennedy Institute of Rheumatology Ethics Committee. Animals were housed in individually ventilated cages at a constant temperature with food and water *ad libitum*. Mice were free of known intestinal pathogens and negative for *Helicobacter* species. C57Bl/6 and $Irf5^{tm1/J}$ (*Irf5*$^{-/-}$) mice were bred in house. C57Bl/6 SJL CD45.1$^{+}$ WT mice were purchased from the University of Oxford BMS. ) $Cx3Cr1^{tm1.1(cre)Jung/J}$, ($CX_3CR1^{IRF5+}$, cWT) were acquired from JAX (Jackson Laboratories, UK, JAX stock #025524)) and crossed with C57BL/6-$Irf5^{tm1Ppr}$/J ($Irf5^{fl/fl}$) to generate conditional *Irf5*$^{-/-}$ mice (cKO, $CX_3CR1^{IRF5-}$). $CX_3CR1^{GFP/GFP}$ CD45.1$^{+}$ mice (B6.129P(Cg)-Ptprc$^{a}$ $Cx3cr1^{tm1Litt/LittJ}$) were maintained in house. B6.SJL-*Ptprc*$^{a}$ (CD45.1$^{+}$ WT mice) were crossed with B6.129P(Cg)-Ptprc$^{a}$ $Cx3cr1^{tm1Litt/LittJ}$ to generate CD45.1$^{+}$ $CX_3CR1^{GFP/+}$, and B6.129P-Cx3cr1tm1Litt/J were crossed with $Irf5^{-/-}$ to generate CD45.2$^{+}$ $CX_3CR1^{GFP/+}$ $Irf5^{-/-}$ mice. For experiments, corresponding strains of mice were co-housed from weaning.

### Generation of Mixed Bone Marrow Chimaeras

≥ 20 g male C57BL/6 SJL (CD45.1$^{+}$ WT) mice were selected as bone marrow recipients. 2 days before irradiation, mice were fed antibiotic-treated water (Co-trimoxazole, Aspen Pharma), or Baytril, Bayer) which was maintained until 2 weeks post-irradiation (PI).

Recipients were lethally irradiated by exposure to 11 Gy split into two equal doses 6 hrs apart in an X-ray irradiator (Gulmay). Within 24 hrs post-irradiation, 4 x$10^6$ freshly isolated bone marrow cells at a 1:1 ratio (CD45.1$^+$ WT and CD45.2$^+$ *Irf5*$^{-/-}$, or CD45.1$^+$ $CX_3CR1^{GFP/+}$ and CD45.2$^+$ $CX_3CR1^{GFP/+}$ Irf5$^{-/-}$) were injected i.v. into the tail vein of CD45.1$^+$ WT hosts. 6 weeks post-irradiation, reconstitution was assessed by collecting blood leukocytes by tail vein bleed.

### *Helicobacter hepaticus* culture

*Helicobacter hepaticus* (Hh) NCI-Frederick isolate 1A (Hh1a; strain 51449; American Type Culture Collection) was grown at 37°C on blood agar plates containing Campylobacter-selective supplement (skirrow), (Oxoid) under microaerophilic conditions (10% $CO_2$, 10% $H_2$, balance $N_2$) in a vented CampyPak jar (Oxoid). After 2 days of blood agar plates, cultures were harvested using cotton swabs and transferred to liquid culture (Tryptan Soya Broth (Sigma Aldrich) dissolved in 1000 mL MilliQ $H_2O$, and autoclaved) containing 10% FCS + 4 mL Campylobacter-selective supplement (skirrow) (Oxoid). Hh culture was inoculated at 0.05 $OD_{600}$ in a 500 mL vented Erlenmeyer flasks (Corning). Liquid culture was maintained at 37°C shaking at 100 rpm under microaerophilic conditions, and split every 24 hours to 0.05 $OD_{600}$ to maintain stable growth. Hh viability was assessed by labelling with a fluorescent live/dead assay kit (Life Technologies) according to the manufacturer's protocol using a CKX41 fluorescence microscope (Olympus).

### *Helicobacter hepaticus* + αIL10R model of colitis

Mice were infected with $1x10^8$ colony forming units (cfu) Hh in 200 µL sterile PBS on days 0 and 1 by oral gavage with a 22G curved, blunted needle (Popper & Sons). Mice were injected intraperitoneally once weekly starting on day 0 with 1 mg anti-IL10R blocking antibody (clone 1B1.2) in a volume of 200 µL. Infected mice were monitored weekly for colitis symptoms. Mice were culled by Schedule 1 method three weeks after day of infection, and organs were harvested for analysis.

### Assessment of bacterial colonisation

Caecal contents were collected after mice were sacrificed. DNA was isolated from faeces using Stool DNA extraction kit (Qiagen) as per manufacturer's instructions. qPCR was performed with primers against the *Hh cdtB* gene using a Viia7 Real-Time PCR system (Applied Biosystems) as described by Maloy *et al.,* (2003) (*58*). In order to construct standard curves, DNA was extracted from Hh cultures using a DNeasy Kit (Qiagen). Primer sequences: *cdt*B Reverse - *TCG TCC AAA ATG CAC AGG TG, cdt*B Forward - *CCG CAA ATT GCA GCA ATA CTT*, *cdt*B Probe - *AAT ATA CGC GCA CAC CTC TCA TCT GAC CAT*.

### qPCR

For each reaction, 10 ng cDNA was added to 2.5 µL 2X qPCR FAST mastermix (Primerdesign). 0.1 µL primer + Taqman probe mix (Table.M2) was added to each

sample, and the reaction volume was topped up to 5 µL with RNase/DNase-free $H_2O$ (Promega). Thermal cycling was carried out using a Viia7 real time PCR system (Applied Biosystems). Thermal cycling: 1x120 s95°C, 40x(5 s 95°C 20 s 60°C).

**Histopathological assessment**

Post-sacrifice, 0.5 cm pieces of caecum, and proximal, mid and distal colon were fixed in PBS + 4% paraformaldehyde (Sigma Aldrich). Fixed tissue was embedded in paraffin blocks, and sectioned using a microtome and stained with Haematoxylin and Eosin (H&E) by the Kennedy Institute of Rheumatology Histology Facility (Kennedy Institute of Rheumatology, University of Oxford).

Sections were scored in a blinded manner by two researchers according to Izcue *et al*., (2008) (*59*).

**Immunofluorescence labelling of colons**

After whole colon excision and longitudinal slicing, colon tissue was washed in PBS, rolled into Swiss rolls, embedded in Optimal Cutting Temperature (OCT) medium (Tissue-Tek), before freezing on dry ice with 2-methylbutane, and stored at -80°C (Bialkowska et al. 2016). 5 µM cryosections were air dried and rehydrated with PBS. The sections were fixed in a 1:1 mixture of methanol:acetone (Merck) and blocked with PBS containing 5% goat serum and 5% mouse serum (blocking solution). Sections were then blocked with biotin/avidin (Invitrogen). Sections were then labelled with primary antibodies (α-F4/80

(recombinant CI:A3-1, Enzo), α-CD11c-biotin (N418, Biolegend), α-CD206 (MR5D3, Bio-rad)) and Sytox blue (Thermo Fisher) performed in blocking solution overnight at 4°C. Secondary antibody labelling was performed with goat α-rat-Alexa Fluor 488, goat α-rabbit-Alexa Fluor 555 and streptavidin-Alexa Fluor 647 (all Thermo Fisher). The sections were stained at RT in the dark for 30 min. Sections were then stained with Hoechst 33342 (Thermo Fisher) for 10min, unless previously stained with Sytox blue overnight. After PBS washes, the tissue was mounted using 5% N-propyl gallate (Merck) in glycerol and imaged using a Zeiss Axio Scope A1 (Zeiss).

**Image analysis and quantification**

The images were analysed using IMARIS (Bitplane). Of each mouse, six individual colon swiss rolls sections were stained in three independent rounds of staining. Within each staining round, intensity thresholds for CD206, CD11c and F4/80 were kept constant. Surfaces were created on F4/80+ cells using the surface tool in Imaris. The size cut-off for a cell was kept at 6.5 µM constantly. Intensity means for CD11c+ and CD206+ cells were defined on single channel spot analysis and kept as a cut-off standard within one staining cycle. Using an automated Python-script, CD11c+ and CD206+ macrophages were defined within F4/80+ cells as cells that reached the intensity mean threshold for CD206 and CD11c respectively. The number of double-positive cells was counted and quantified as a percentage of total F4/80+ cells. For quantification of macrophage subsets distance to the epithelium, a region of interest within one swiss roll was selected based on tissue architecture where the different regions (epithelium, lamina propria and muscularis) across the depth of the colon were clearly visible. Using the filaments tool,

the epithelium and serosal membrane were manually drawn and a channel was created using these filaments. Surfaces were created automatically on these channels, and using the distance transformation tool within the surface statistics, two channels were created that measured the distance of a selected object in relation to their surface. Again, F4/80+ cell surface statistics and defining CD206+ and CD11c+ macrophages were analysed as described above. In addition, each CD206+ and CD11c+ macrophage was set in relation to its minimal distance to the epithelium and the serosal membrane using the distance transformation channels described above. Adding the two minimal distances for each macrophage gives the total distance between the membranes for each point. Distance to membrane was calculated as a percentage of the minimal distance of the respective membrane in relation to the total membrane, allowing correction for the elongation of the epithelium in inflammation.

**Isolation of lamina propria leukocytes**

Colons and/or caeca were harvested from mice, washed in PBS/BSA and content flushed with forceps. Intestines were then opened longitudinally and washed once more before blotting to remove mucus. Gut tissue was then cut into 1 cm long pieces and placed in 50 mL centrifuge tube (Greiner) in ice cold PBS + 0.1% BSA. Colons were incubated 2 times at 200 rpm in 40 mL HBSS + 0.1% BSA + 1% Penicillin-Streptomycin (PS, Lonza) + 5mM EDTA (Sigma-Aldrich) at 37 °C for 10 min before the supernatant was aspirated. Tissue was placed in 40 mL PBS + 0.1% BSA + 1% PS for 5 min. Intestines were then incubated with 20 mL RPMI + 10% FCS +1% PS + 2.5 U/mL Collagenase VIII (Sigma-Aldrich) + 2 U/mL DNAse I (Roche), shaking at 200 rpm for 45 mins - 1 hour at 37 °C. Supernatant

was filtered through a 70 μm cell strainer to which 30 mL of ice cold PBS + 0.1% BSA + 1% PS + 5 mM EDTA was added to ablate collagenase/DNase activity. Cells were washed in 30 mL PBS/BSA before filtering once more through a 40 μm cell strainer. The cells were then pelleted by centrifugation at 400 rcf for 10 minutes at 4 °C.

Colonic lamina propria leukocytes (cLPLs) were isolated by resuspending cells in 4 mL P80 (80% P100 (9:1 percoll:10X PBS) + 20% RPMI) percoll in a 15 mL centrifuge tube (Greiner) before overlaying 4 mL P40 (40% P100 + 60% 1X PBS) layer. Cells were spun at 3000 rpm for 20 min at room temperature, slow acceleration, no brake. Mucus and cellular debris were aspirated from the surface of the P40 layer with a Pasteur pipette and pipetted into 40 mL of ice cold PBS + 0.1% BSA. Cells were pelleted by centrifugation at 400 rcf for 10 min and resuspended in 1 mL RPMI + 10% FCS + 1% PS before counting.

**Isolation of blood leukocytes**

Blood was harvested by either tail vein bleed or cardiac puncture. Mice were culled by Schedule 1 method in accordance with the project licence. Prior to cardiac puncture a 1 mL syringe was coated with PBS + 2 mM EDTA. Cardiac puncture was performed with a 27G needle. Tail vein bleeds were performed using a #24 blade scalpel (Swann-Morton Ltd.) Collected blood was placed in 1 mL of sterile 2 mM EDTA/PBS solution in a 15 mL centrifuge tube (Greiner). Tubes were topped up with ice-cold PBS + 0.1% BSA. Cells were pelleted by centrifugation at 400 rcf for 10 mins at 4 °C and the supernatant discarded. Erythrocytes were then lysed using 10-20X the blood sample volume of ACK lysis buffer (Gibco) for 3 mins. Tubes were then topped up to 15 mL with ice cold PBS +

0.1% BSA to quench the lysis buffer. Cells were washed in PBS/BSA, resuspended in PBS + 0.1% BSA to the desired cell concentration, and stored at 4 °C until required.

**Bone marrow isolation**

Whole hind legs of mice were harvested and stored at 4 °C until processing. Processing was carried out in a class II lamina flow hood. Femurs and tibia muscle tissue was removed using scissors, followed by desiccation in 70% ethanol solution for 3 min. Remaining muscle was cleaned from the bones using a lint-free tissue. Scissors were used to cut the ends of bones. A 27G needle was inserted into the opening, and marrow was flushed into a 50 mL centrifuge tube using 10 mL of sterile, ice cold PBS. Cells were then filtered through a 70 µm cell strainer (Greiner). Red blood cells were lysed with ACK as described above. Cells were resuspended in PBS + 0.1% BSA at 4 °C until required.

**Monocyte isolation**

Splenocytes were prepared as described above. Monocytes were enriched by negative selection using an EasySep™ Mouse Monocyte Isolation Kit (StemCell) according to the manufacturer's instructions. Cells were then resuspended in ice cold PBS + 0.1% BSA for counting and downstream processing.

**T cell restimulation**

A minimum of 1 x$10^6$ freshly isolated cLPLs were incubated in V-bottomed 96 well plates (Corning) in 250 µL Iscove's Modified Dulbecco's Medium (Gibco) supplemented with 10% FCS + 1% P/S + 0.1 µM phorbol 12-myristate 13-acetate (PMA, Sigma Aldrich) + 1µM Ionomycin (Sigma Alrich) + 10 µg/mL GolgiPlug (BD) for 4 hrs at 37 °C. Cells were washed 3 x in 150 µL FACS buffer before extracellular and intracellular staining.

**Flow cytometry**

CompBeads (BD) were used to prepare single stained controls as per manufacturer's instructions to set up fluorophore compensation. Labelled cells were acquired using either an LSR II (BD), or Fortessa X20 (BD) flow cytometer using FACSDiva (BD). Data were analysed using Flowjo (Treestar, Inc.) software.

**Extracellular labelling of cells**

5x$10^5$ - 2x$10^6$ cells were plated on either V-bottomed or U-bottomed 96 well plates. The cells were washed twice with 150 µL FACS buffer (PBS + 0.1 % BSA + 1 mM EDTA + 0.01% Sodium Azide) at 400 rcf for 3 min 4°C. Cells were then Fc blocked for 10 min with αCD16/CD32 (BD) 1/100 in 20 µL FACS buffer at room temperature (RT) followed by washing once in 150 µL FACS buffer. Fixable Viability Dye eFluor®780 (ThermoFisher) and primary extracellular antibodies (**Table. 1**) were added for 20 min at 4 °C in 20 µL FACS buffer in the dark. Labelled cells were then washed twice with 150 µL FACS buffer. Cells were then fixed for 30 mins in 50 µL Cytofix (BD), washed twice with 150 µL FACS buffer, and resuspended in 200 µL FACS buffer before acquisition. For assessment of

apoptosis, the eBioscience™ Annexin V Apoptosis Detection Kit APC (ThermoFisher) was used according to manufacturer's instructions in combination with extracellular labelling and fixable viability dye.

**Intracellular labelling of cytokines**

Intracellular labelling of cytokines from mouse colons was performed immediately after isolation without further stimulation. Surface markers were labelled as described above. For Cytokine labelling, cells were fixed in 50 µL Cytofix/Cytoperm (BD), washed twice in 150 µL Perm/Wash buffer (BD) at 600 rcf, 4 °C. Intracellular antibodies (**Table. 2**) were incubated in 20 µL Perm/Wash for 20 mins at 4 °C in the dark, after which samples were washed twice in 150 µL Perm/Wash, and once in 150 µL FACS buffer before resuspension in 200 µL FACS buffer for acquisition.

**Intracellular labelling of IRF5**

Intracellular labelling of IRF5 was performed immediately after isolation without further stimulation. Surface markers were labelled as described above. For nuclear staining, cells were fixed in 50 µL Fix/Perm (eBioscience) according to manufacturer's instructions, washed twice in 150 µL Perm buffer (eBioscience) at 600 rcf, 4 °C. Intracellular antibodies (**Table. 2**) were incubated in 20 µL Perm for 20 mins at 4 °C, protected from light. Next, samples were washed twice in 150 µL Perm, and once in 150 µL FACS buffer before resuspension in 200 µL FACS buffer for acquisition.

**Cell sorting**

Cells were stained with extracellular cytokines as described above, except no fixation step was performed. Cells were then sorted using a FACSAria™ II (BD) at the Kennedy Institute of Rheumatology FACS facility.

**Generation and analysis of "small bulk" RNA-sequencing data from MBMC**

For "small bulk" RNA-sequencing 100 cell samples were sorted through a 100 µm diameter nozzle into 2 µL of lysis buffer and amplified cDNA prepared using the Smart-seq2 protocol (*60*). Libraries were prepared using Nextera XT kits (Illumina) and sequenced to a mean depth of 17M read pairs (Illumina HiSeq 4000). Sequence reads were aligned to the mouse genome with Hisat2 (version 2.1.0) using a "genome_trans" index built from the mm10 release of the mouse genome and Ensembl version 91 annotations (two-pass strategy to discover novel splice sites; with parameters: --dta and --score-min L,0.0,-0.2) (*61*). Mapped reads were counted using featureCounts (Subread version 1.6.3; Ensembl version 91 annotations; default parameters) (*62*). TPMs were estimated with salmon (version 0.11.3, with parameter "--gcBias") using a quasi index built from the full set of Ensembl version 91 transcriptome annotations (parameters "--k=31 --keepDuplicates") (*63*). The median alignment rate was 83.8% (assessed with Picard tools v2.10.9, https://github.com/broadinstitute/picard).

For each of the GSEA analyses genes detected in a least one of the biological replicates (n=3) were pre-ranked by p-value for differential expression (Deseq2, paired design, local

fit for dispersion, no independent filtering). Enrichment of GO biological processes (org.Mm.ed.db R package version 3.7.0; with ≥5 and ≤500 genes) was tested using fgsea (*64*) (version 1.8.0). Changes in gene expression across the wildtype monocyte waterfall were identified using DESeq2 (likelihood ratio test, modelling animal and cell-type). Differential expression analyses were performed using DESeq2 (paired tests, local dispersion fit).

**Generation and pre-processing of single-cell RNA-sequencing data**

The inflamed cLP small-bulk RNA-seq and scRNA-seq data were generated from a common set of MBMCs (n=3, cells pooled from all animals for scRNA-seq analysis). Subsequently, in a separate experiment, the steady state blood and cLP scRNA-seq datasets were generated from a second set of MBMCs (n=5, cells pooled from all animals for both analyses). Single-cell RNA-sequencing libraries were generated using the 10x Genomics Single Cell 3' Solution (inflamed colon dataset: version 2; steady state colon and PBMC datasets: version 3) kit and sequenced (inflamed colon dataset: Illumina HiSeq 4000 with an average depth of >200k read per cell; steady state colon and PBMC datasets: NovaSeq 6000 with an average depth of >50k reads per cell). Data analysis was performed using Python3 pipelines (https://github.com/sansomlab/tenx) written using CGAT-core[75]. Read mapping, quantitation and aggregation of sample count matrices was performed with the 10x Genomics Cell Ranger pipeline (inflamed colon dataset: version 2.1.1; steady state datasets: version 3.1.0). For the "cellranger count" step, a custom reference was built using Ensembl annotations (version 91) that included genes with protein coding, lincRNA, macro_lincRNA, immune (IG_*, TR_*), antisense_RNA, and

miRNA Ensembl (version 91) biotypes. Within each dataset, *Irf5*$^{-/-}$ and wildtype samples were aggregated. No normalisation was applied during the aggregation step. Cells with barcodes common to more than one sample from the same sequencing batch were removed from the analysis to avoid issues associated with index hopping. For each of the three experiments, the aggregated count matrices were randomly down-sampled in order to normalise the median number of UMIs per-cell between the *Irf5*$^{-/-}$ and wildtype samples ("downsampleMatrix" function from the DropletUtils R package) and genes detected in less than 3 cells removed.

For the inflamed colon dataset, cells with < 500 genes, > 30k UMIs, < 0.3% or > 7.5% mitochondrial UMIs or that were identified as contaminating B cells (n=38) were removed. For the steady state colon dataset, cells with < 1k genes, > 25k UMIs, > 7.5% mitochondrial UMIs, identified as contaminating B, T or stromal cells (n=75), or with high expression of interferon-induced genes (n=34) were removed. For the steady state PBMC dataset, cells with < 500 genes, > 20k UMIs, > 5% mitochondrial UMIs, with high expression of haemoglobin genes (n=8) or identified as contaminating T cells (n=694) were removed. For each of the datasets either the WT or Irf5$^{-/-}$cells were randomly down sampled to retain an equal number of cells per genotype.

**Analysis of single-cell RNA-sequencing data from the inflamed cLP**

Per-cell UMI counts were normalised, scaled and variation associated with total UMI counts, percentage of mitochondrial counts and cell cycle (all effects; using known G2 and S phase associated genes (*66*)) regressed out with the Seurat R package (version 2.3.4). Significantly variable genes were selected using the “trendVar” function from the R Bioconductor package Scran (minimum mean log-expression 0.05, BH adjusted p-

value < 0.05). These genes were used as input for principal component analysis (PCA), and significant PCs (n=30) identified using Seurat ("JackStraw" test, BH adjusted p < 0.05). Graph-based clustering of the significant PCs was performed using Seurat ("original" Louvain algorithm, resolution=1.1). Significant cluster markers conserved between the genotypes were identified by intersecting the results of separate tests for cluster markers within each genotype (Seurat "Findmarkers" function, Wilcoxon tests, BH adjusted p value < 0.05). The UMAP projection was computed using all of the significant PCs ("RunUMAP" function, Seurat). Significant differentially expressed genes between genotype within cluster were identified using the "FindMarkers" function (Wilcoxon tests, BH adjusted p value < 0.05, fold change > 1.5).

For pseudo-time analysis the data was subset to cells identified as Monocytes or Macrophages. Significant variable genes and PCs (n=20) and clusters (resolution=1.2) were recomputed as above. The diffusion map (Figure 6a) was constructed from all of the significant PCs using the R Destiny package[77]. The R package Slingshot (version 1.2.0) was used to fit a minimum spanning tree to the full diffusion map and to infer the global lineage structure ("*Ly6c2* mono" cluster specified as the root state) [45]. Slingshot was used to construct smoothed curves along the lineages and to compute pseudo-time values for each cell.

**Analysis of steady state blood and cLP single-cell RNA-sequencing datasets**

These datasets were analysed using Seurat version 3.1.1. Normalisation was performed with sctransform (default parameters), and variation associated with mitochondrial UMI

percentage or cell cycle (all effects; using known G2 and S phase associated genes[76]) regressed out. Principal components were calculated using the top 3,000 variable features. Clustering was performed with the Leiden algorithm (cLP dataset: k=30, n=30 top PCs, resolution=1; PBMC dataset: k=30, n=15 PCs, resolution=0.25). Significant cluster markers and genes differentially expressed between genotype within cluster were identified as described for the inflamed cLP dataset.

**Statistical analysis**

Data were analysed using Prism V.7 (GraphPad). Statistical tests were performed as indicated in figure legends. Two-sided testing was used in all instances unless indicated. Differences were considered statistically significant when $p \leq 0.05$.

## Supplementary Figures and Tables

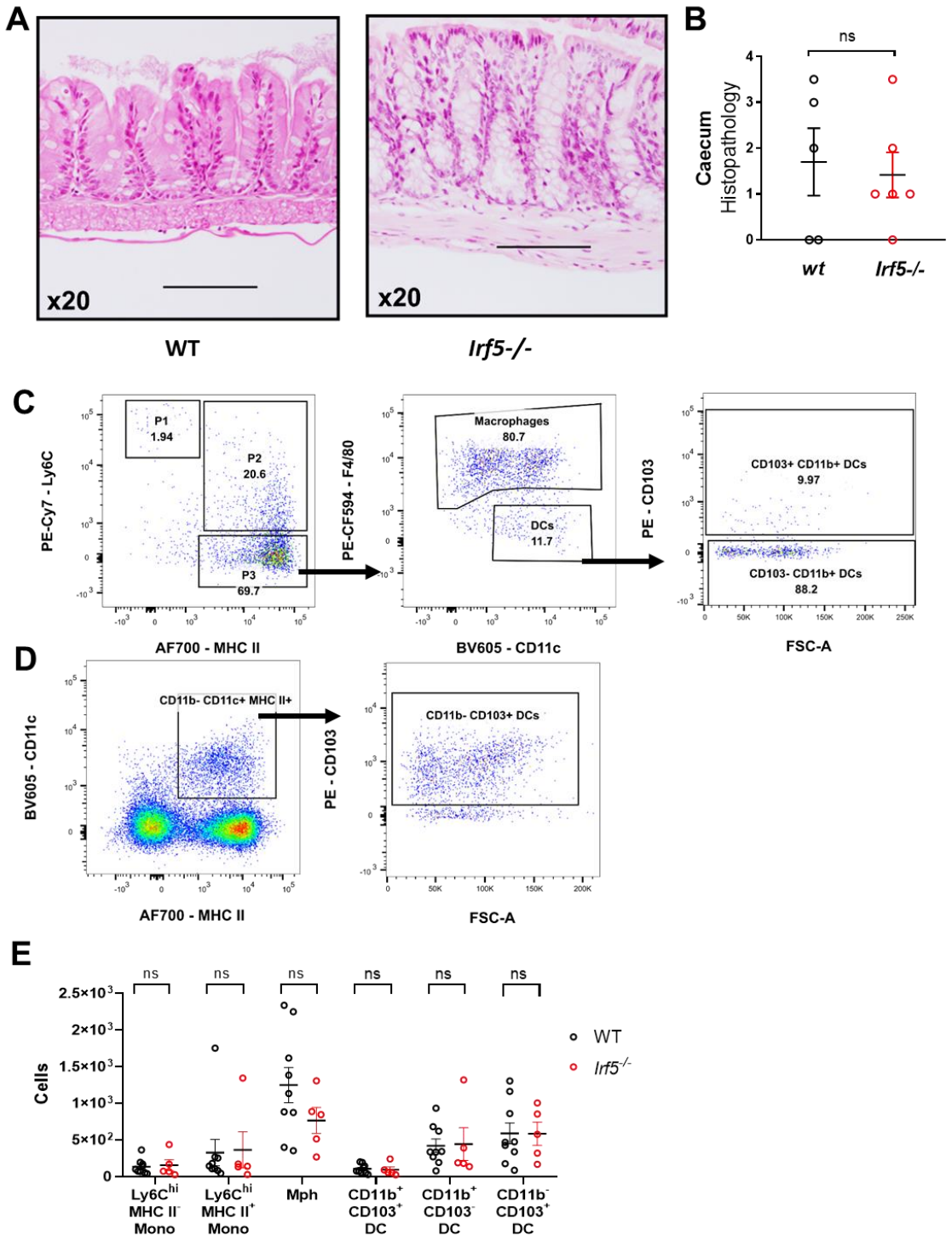


**Supplementary Figure S1: IRF5 deficiency and caecum physiology at steady state. A)** H&E sections of WT (n=5) and *Irf5*$^{-/-}$ (n=5) caecum at steady state. **B)** Histopathology scoring of steady

state caeca. **B, C)** Mann-Whitney U test **C)** Gating strategy to identify P1 monocytes, P2 monocytes, macrophages, and CD11b$^{+}$ CD103$^{+}$ DCs and CD11b$^{+}$ CD103$^{-}$ DCs representative of steady state mice. **D)** Gating strategy for CD11b$^{-}$ CD103$^{+}$ DCs. **C, D)** Gating done on LiveCD45$^{+}$Dump$^{-}$CD11b$^{+}$Ly6G$^{-}$SiglecF and was based on FMO controls. **E)** The absolute number of intestinal MNPs in the cLP of steady state WT (n=9) and *Irf5*$^{-/-}$ (n=5) mice. Two-Way ANOVA with Sidak correction. **B, C, E)** Mann-Whitney U test. Data presented are mean ± SEM, ns = not significant.

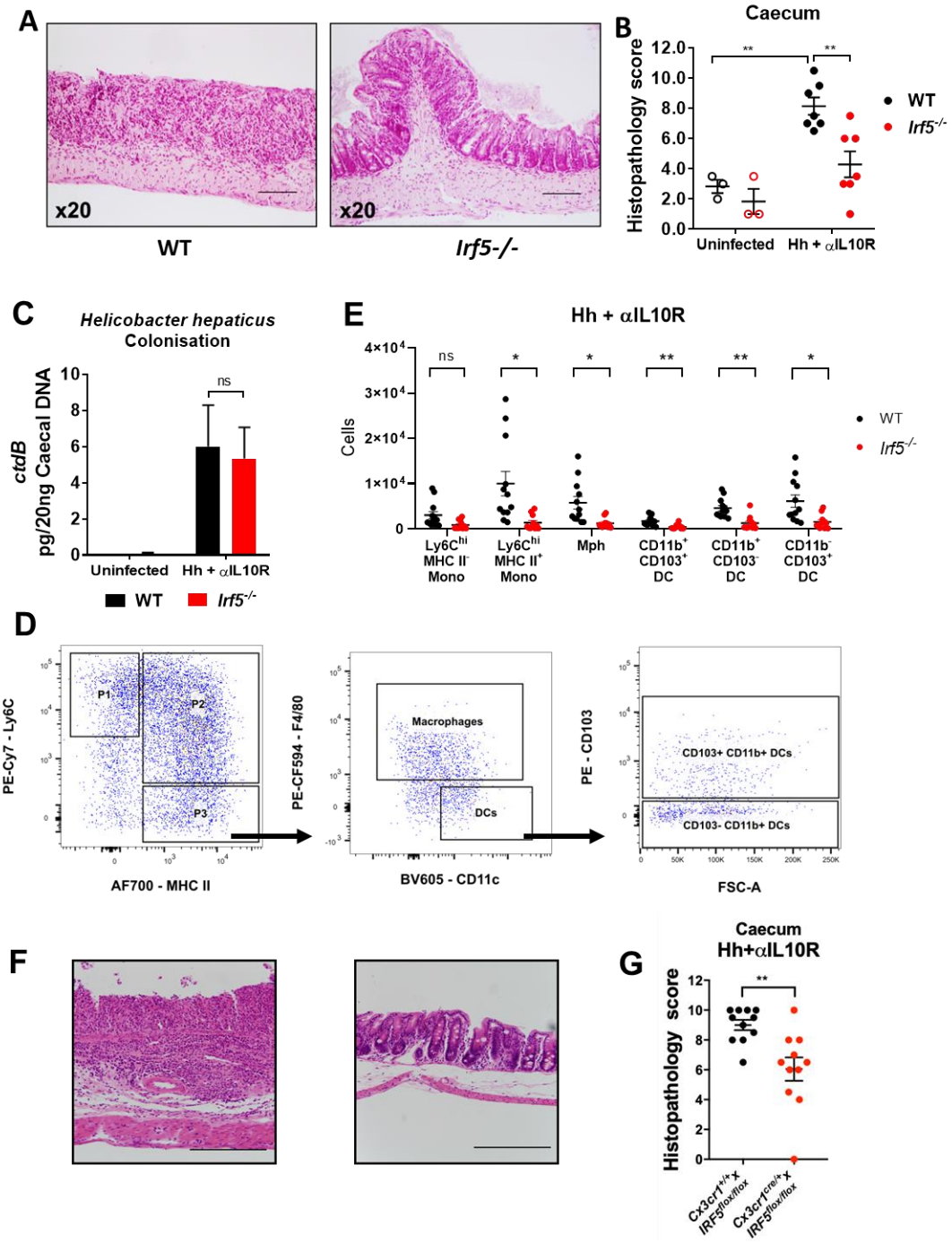

**Supplementary Figure S2: IRF5 deficiency and caecum in inflammation. A)** Representative of two independent experiments H&E-stained sections of WT and *Irf5*$^{-/-}$ caecum at d21 Hh + αIL10R colitis. **B)** Histopathology scoring of inflamed caeca (WT ss n= 3 and Hh n =7, *Irf5*$^{-/-}$ ss n= 3 and Hh n =7). **C)** Quantification of *Helicobacter hepaticus* load at d21 colitis (WT ss n= 3 and Hh n =7, *Irf5*$^{-/-}$ ss n= 3 and Hh n =7. **D)** Gating strategy to identify P1 monocytes, P2 monocytes, macrophages, and CD11b$^{+}$ CD103$^{+}$ DCs and CD11b$^{+}$ CD103$^{-}$ DCs representative of d21 Hh + αIL10R inflamed mice. Gating done on LiveCD45$^{+}$Dump$^{-}$CD11b$^{+}$Ly6G$^{-}$SiglecF and was based on FMO controls. **E)** The absolute number of intestinal MNPs in the cLP of WT (n=12) and *Irf5*$^{-/-}$ (n=11) mice at d21 colitis. Data are pooled from two independent experiments. Two-Way ANOVA with Sidak correction. **F)** Representative H&E stained sections of CX$_3$CR1$^{IRF5+}$ or CX$_3$CR1$^{IRF5-}$ caeca at d21 colitis. **G)** Histopathology scoring of CX$_3$CR1$^{IRF5+}$ and CX$_3$CR1$^{IRF5-}$ mice at d21 Hh + αIL10R colitis (WT n=12, *Irf5*$^{-/-}$ n=12). Data presented are mean ± SEM, ns = not significant, * p ≤ 0.05, ** p ≤ 0.01, *** p ≤ 0.001, **** p < 0.0001

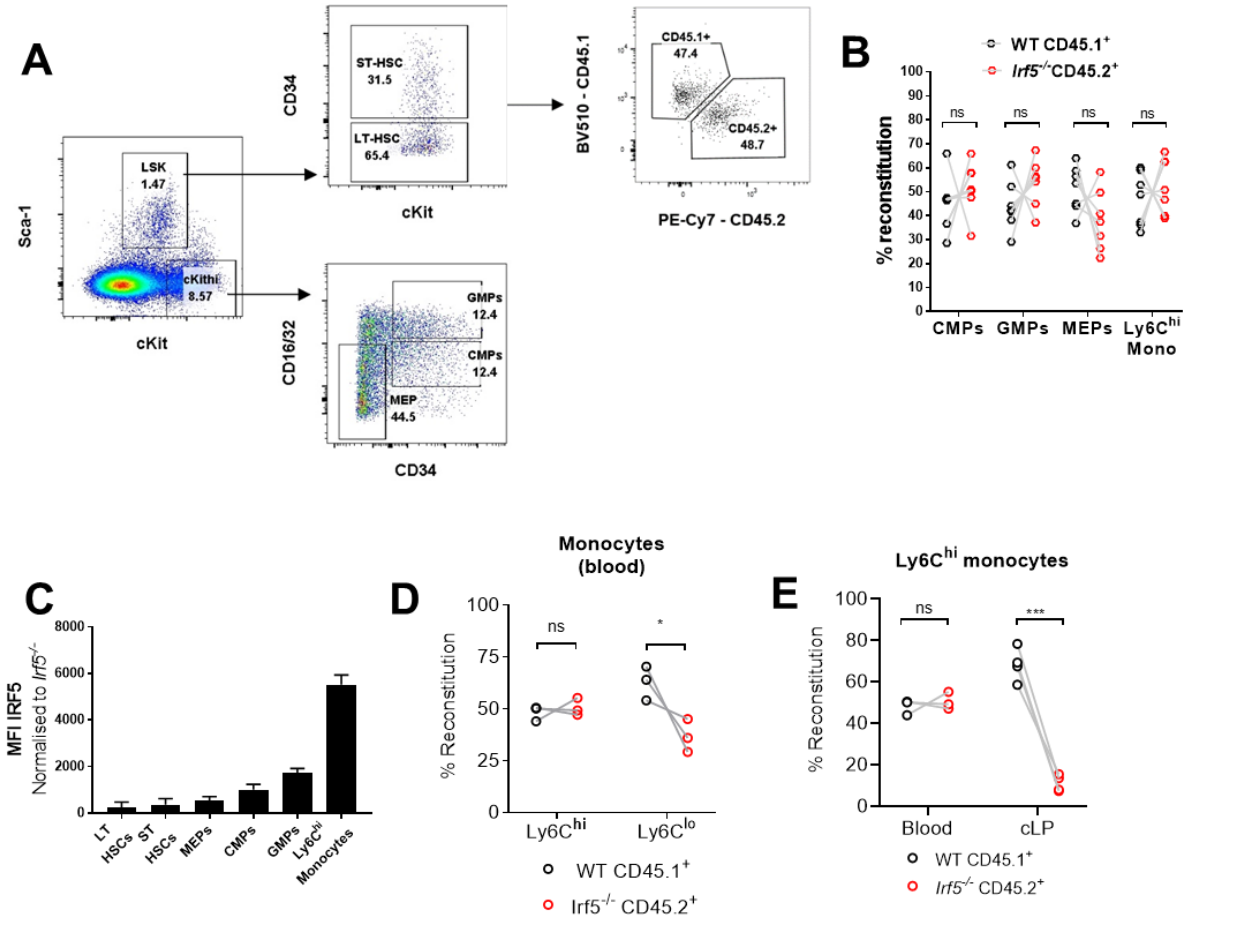


**Supplementary Figure S3: MBMC: monocyte development in the bone marrow and blood.** **A)** Gating strategy to identify HSPCs in MBMC. **B)** Quantification of HSPC reconstitution (n=7). **C)** IRF5 expression in the bone marrow quantified by intracellular flow cytometry staining. **D)** Reconstitution of blood Ly6C$^{hi}$ and Ly6C$^{lo}$ monocytes (n=3). **E)** Reconstitution of blood and cLP Ly6C$^{hi}$ monocytes (n=3-5).

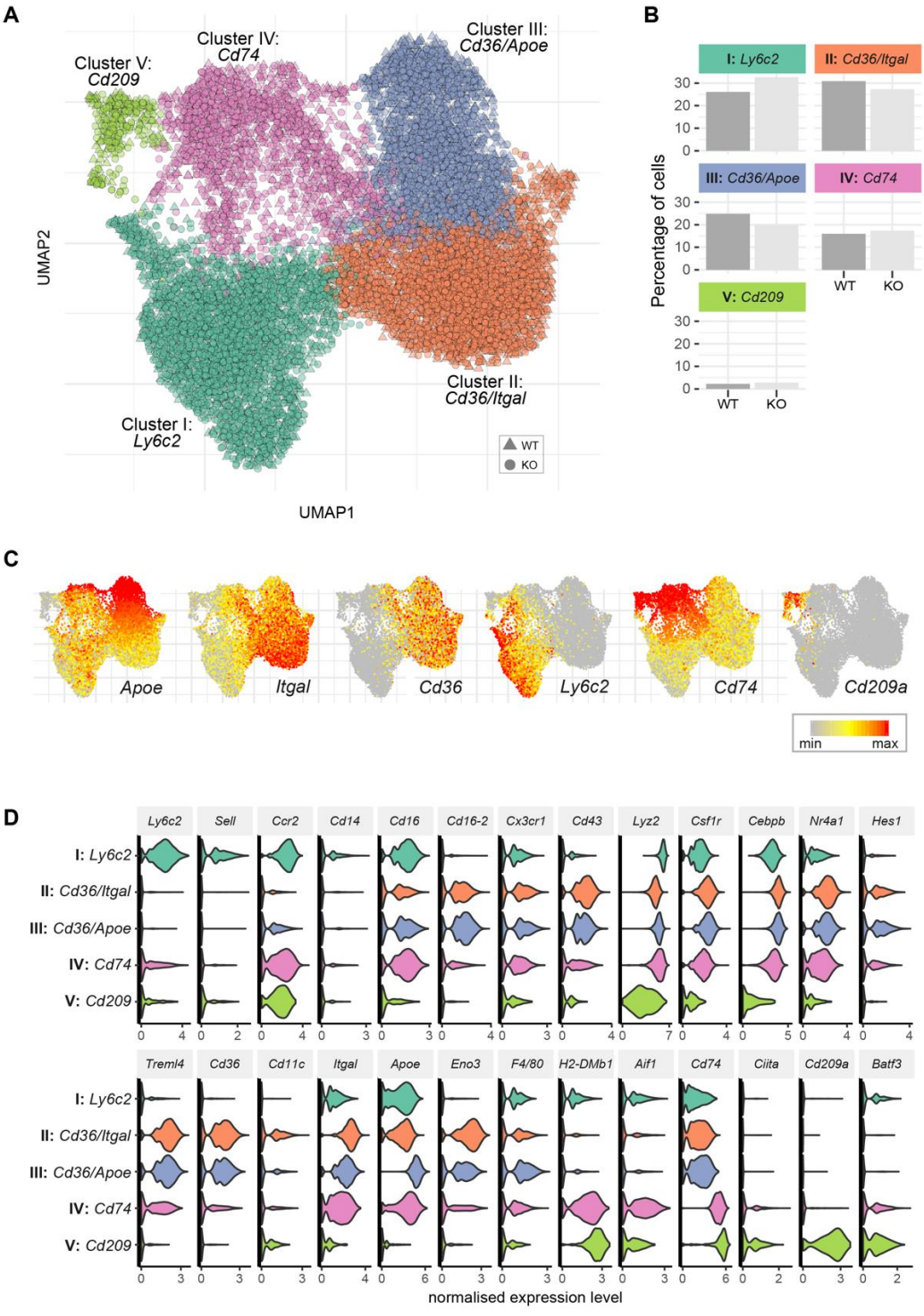


**Supplementary Figure S4: scRNA-seq: monocyte development in blood**. CD45$^{+}$CD11b$^{+}$ SiglecF$^{-}$Ly6G$^{-}$CX$_3$CR1$^{+}$Dump- cells were sorted from the blood of five MBMC animals and

subjected to droplet-based single cell transcriptomic analysis. **A)** Graph based clustering[76] of equal numbers of WT and *Irf5*$^{-/-}$ cells (n=12528 total) identified five monocyte clusters. **B)** The bar plots show the percentages of WT and *Irf5*$^{-/-}$ cells that were found in each cluster. **C)** The expression of selected genes that mark the identified populations. **D)** The violin plots show the expression levels (x axes) of selected markers of monocyte sub-populations in each of the identified clusters (y axes).

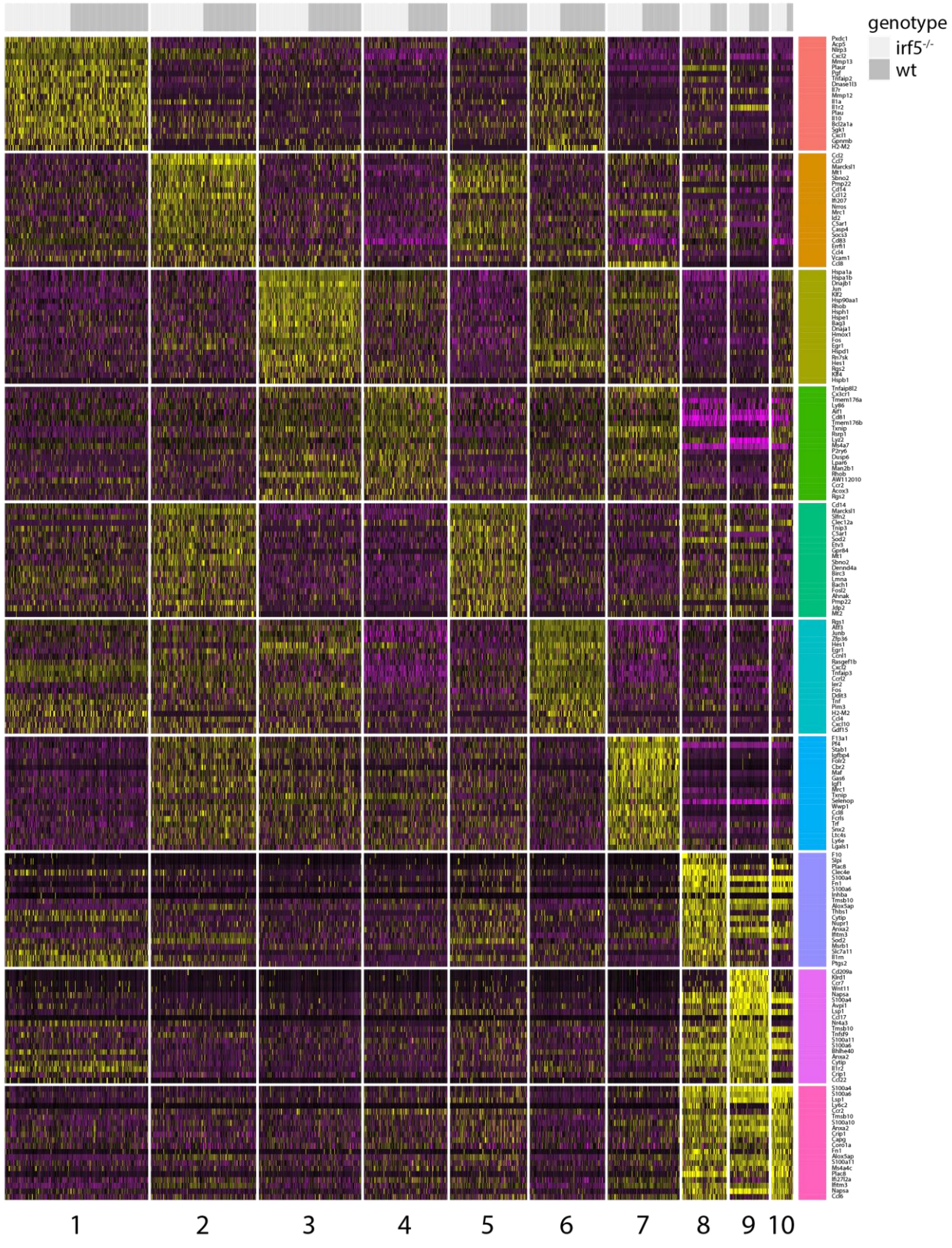
genotype
irf5-/-
wt
1
2
3
4
5
6
7
8
9
10

**Supplementary Figure S5: scRNA-seq: MNP populations in cLP at steady state.** The heatmap shows the expression of the top significant conserved cluster marker genes from the MBMC single-cell RNA-sequencing experiment (**Fig 3**) (Seurat analysis, Wilcoxon tests, BH adjusted $p < 0.05$ in separate tests of cells of both genotypes). scRNA-seq: experiment performed once, pool of MNPs isolated from cLP of 5 MBMCs.

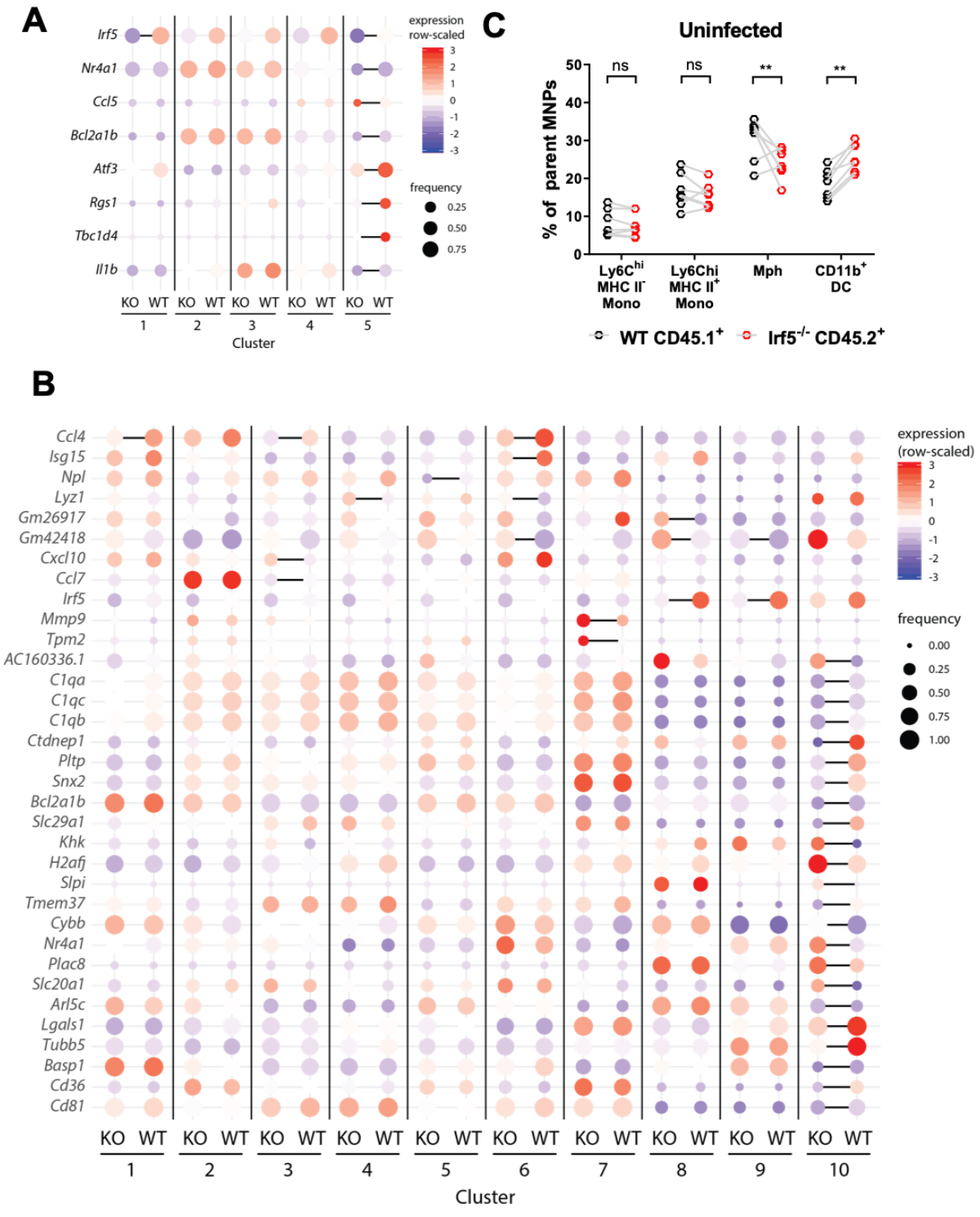


**Supplementary Figure S6: scRNA-seq: IRF5 effect on blood monocytes and cLP MNPs at steady state**. The split dot plots show within cluster differential expression between steady state WT and *Irf5*$^{-/-}$ **A)** blood monocytes (see **Supplementary Fig S4**) and **B)** cLP MNP (see **Fig 4**). Significant differences between the genotypes (|fc| > 1.5, BH adjusted $p < 0.05$, Wilcoxon tests) are indicated by solid black lines. All genes found to be significantly differentially

expressed in at least one cluster are shown. Dot size is proportional to the frequency of gene detection in the single cells. Dot colour is proportional to the (row-scaled) expression level of the gene. **C)** The relative compositions of the MNP compartment of WT- and *Irf5*$^{-/-}$-donor derived cLPLs were analysed by flow cytometry in uninfected MBMCs. Data are pooled from two independent experiments. Two-Way ANOVA with Sidak correction. Data presented are mean ± SEM, ns = not significant, ** p ≤ 0.01, *** p ≤ 0.001, **** p < 0.0001.

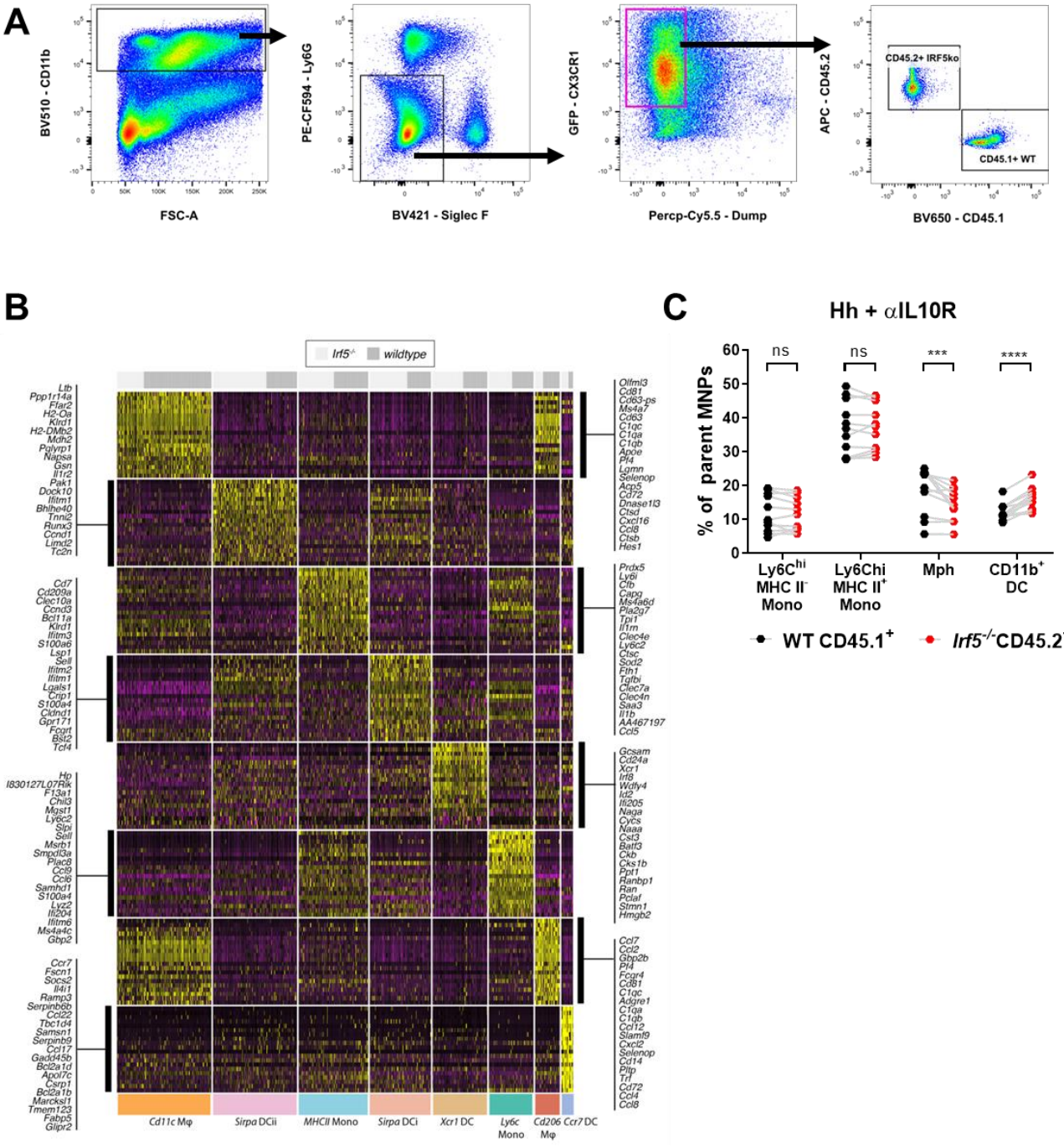

**Supplementary Figure S7: scRNA-seq: MNP populations in inflamed colon. A)** Representative gating strategy for sorting $CX_3CR1^+$ MNPs from MBMCs, gated on singlets, Live, $CD45^+$. **B)** The heatmap shows the expression of the top significant conserved cluster marker genes from the MBMC single-cell RNA-sequencing experiment (Seurat analysis, Wilcoxon tests, BH adjusted $p < 0.05$ in separate tests of cells of both genotypes). scRNAseq: experiment performed once, pool of MNPs isolated from cLP of 3 MBMCs at d21 Hh + αIL10R colitis. **C)** The relative compositions of the MNP compartment of WT- and *Irf5*$^{-/-}$-donor derived cLPLs were analysed by flow cytometry in MBMCs at d21 Hh + αIL10R colitis. Data are pooled from two independent experiments. Two-Way ANOVA with Sidak correction. Data presented are mean ± SEM, ns = not significant, ** $p \leq 0.01$, *** $p \leq 0.001$, **** $p < 0.0001$.

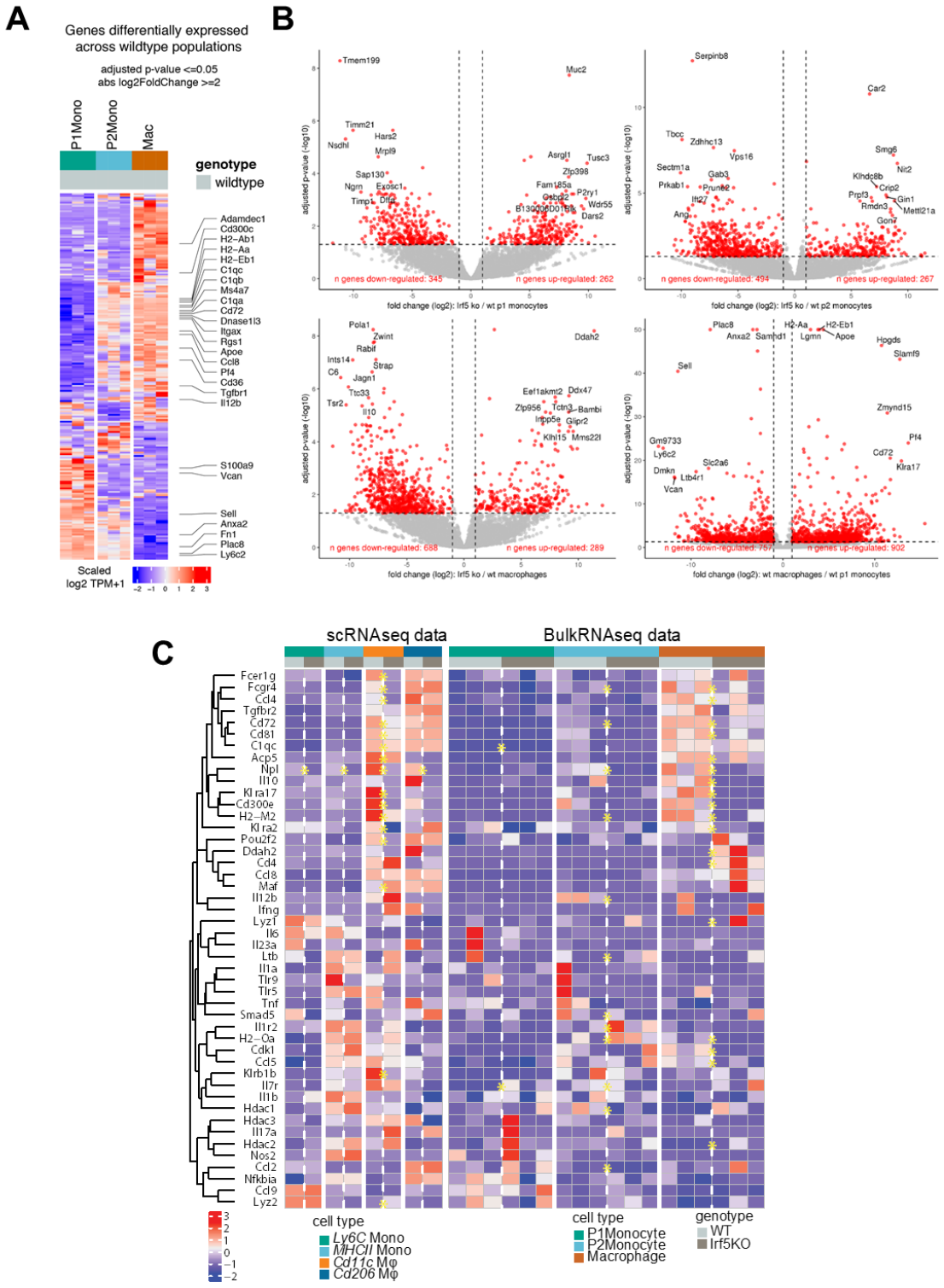


**Supplementary Figure S8: scRNA-seq and bulk RNA-seq: comparison of IRF5 dependent genes.** Small-bulk RNA-seq analysis of MNP populations at d21 Hh + αIL10R colitis (experiment performed once, n=3 chimaeras)**. A)** The heatmap shows the expression of genes with significant variation in expression between WT P1 monocytes, WT P2 monocytes and WT macrophages isolated from the inflamed cLP of the MBMCs (DESeq2, LRT test, BH adjusted p

< 0.05). **B)** The volcano plots show genes found to be significantly differentially expressed (red dots, separate DESeq2 analyses, BH adjusted p < 0.05, | fc | >2) between WT vs *Irf5*$^{-/-}$ P1 monocytes (top left), WT vs *Irf5*$^{-/-}$ P2 monocytes (top right), WT vs *Irf5*$^{-/-}$ macrophages (bottom left), and between WT P1 monocytes vs WT macrophages (bottom right). **C)** The heatmap shows expression of genes found to be significantly differentially expressed (yellow stars, BH adjusted p < 0.05) between WT and *Irf5*$^{-/-}$ MNPs in scRNA-seq (Wilcoxon tests) or small bulk RNA-seq (DESeq2 analyses) datasets.

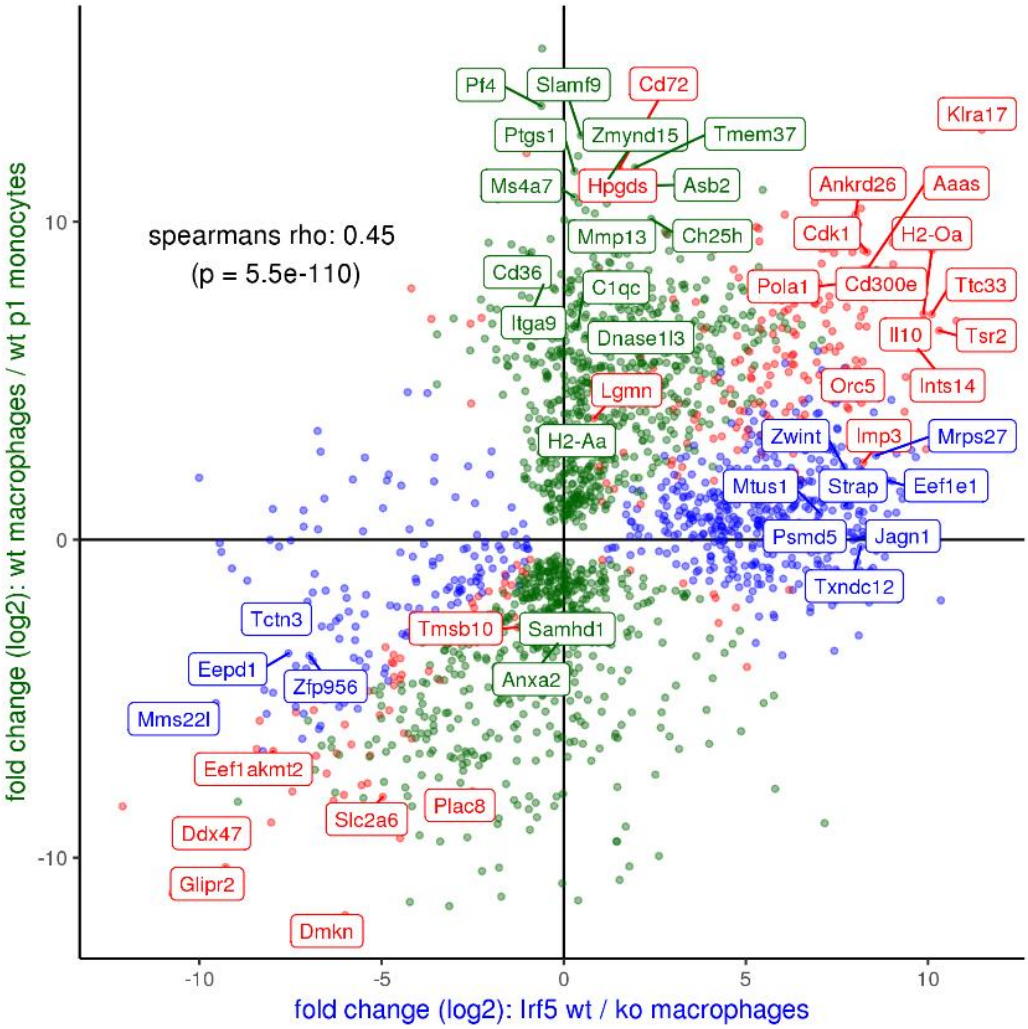


**Supplementary Figure S9: IRF5 in monocyte to macrophage differentiation.** Comparison of genes differentially expressed in WT vs *Irf5*$^{-/-}$ macrophages with those differentially expressed between WT P1 monocytes and WT macrophages isolated from d21 Hh + αIL10R MBMCs. Genes are coloured to indicate significant differential expression in both comparisons (red dots), in only WT vs *Irf5*$^{-/-}$ macrophages (blue dots) or in only WT P1 monocytes vs WT macrophages (green dots) (DESeq2 analyses, BH adjusted p < 0.05, see **Supplementary Fig. S6b**).

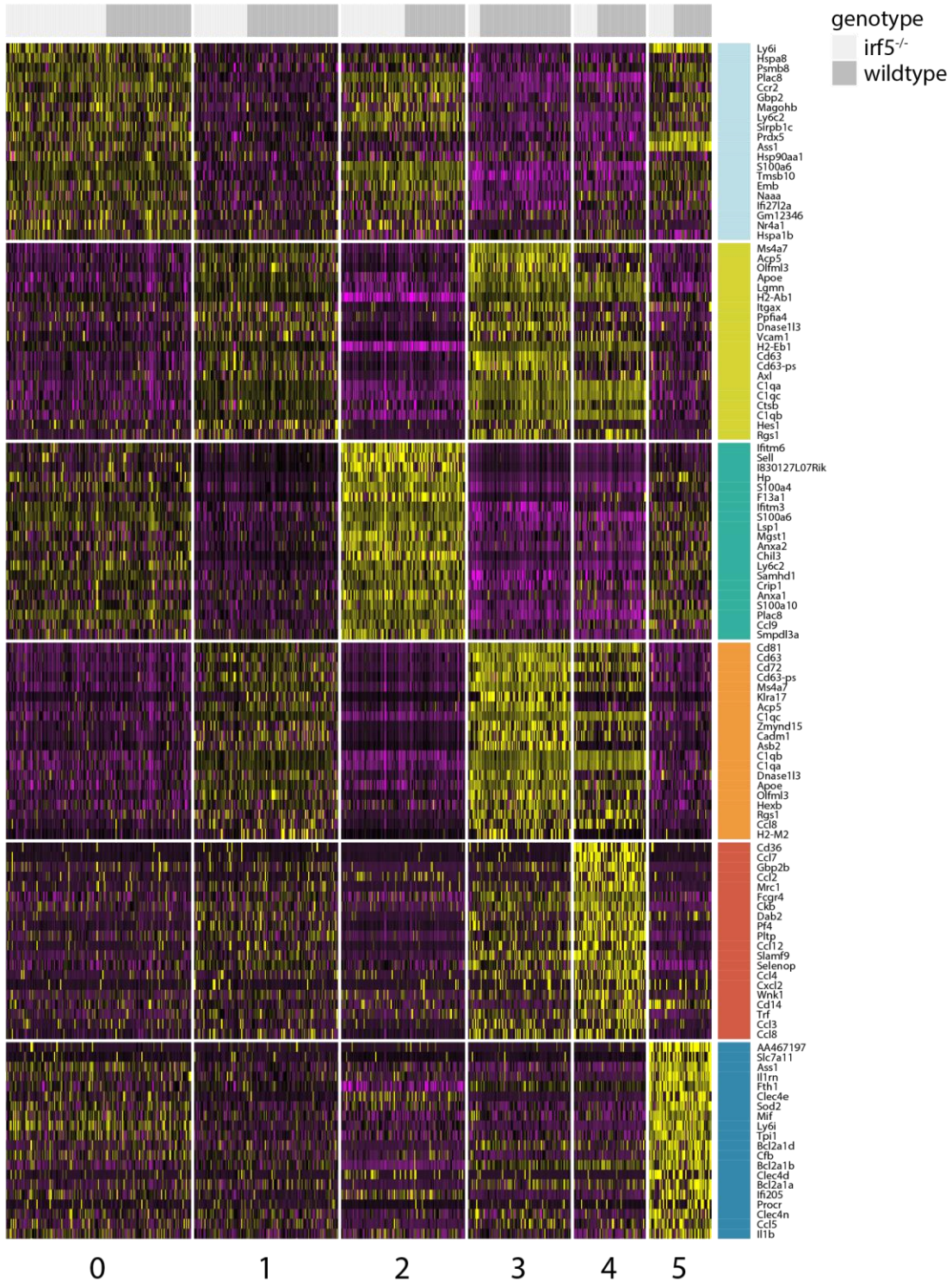


**Supplementary Figure S10: scRNA-seq: monocyte and macrophage populations in inflamed colon.** The heatmap shows the expression of the top significant marker genes for the clusters shown in **Fig 6** (Seurat analysis, Wilcoxon tests, BH adjusted $p < 0.05$).

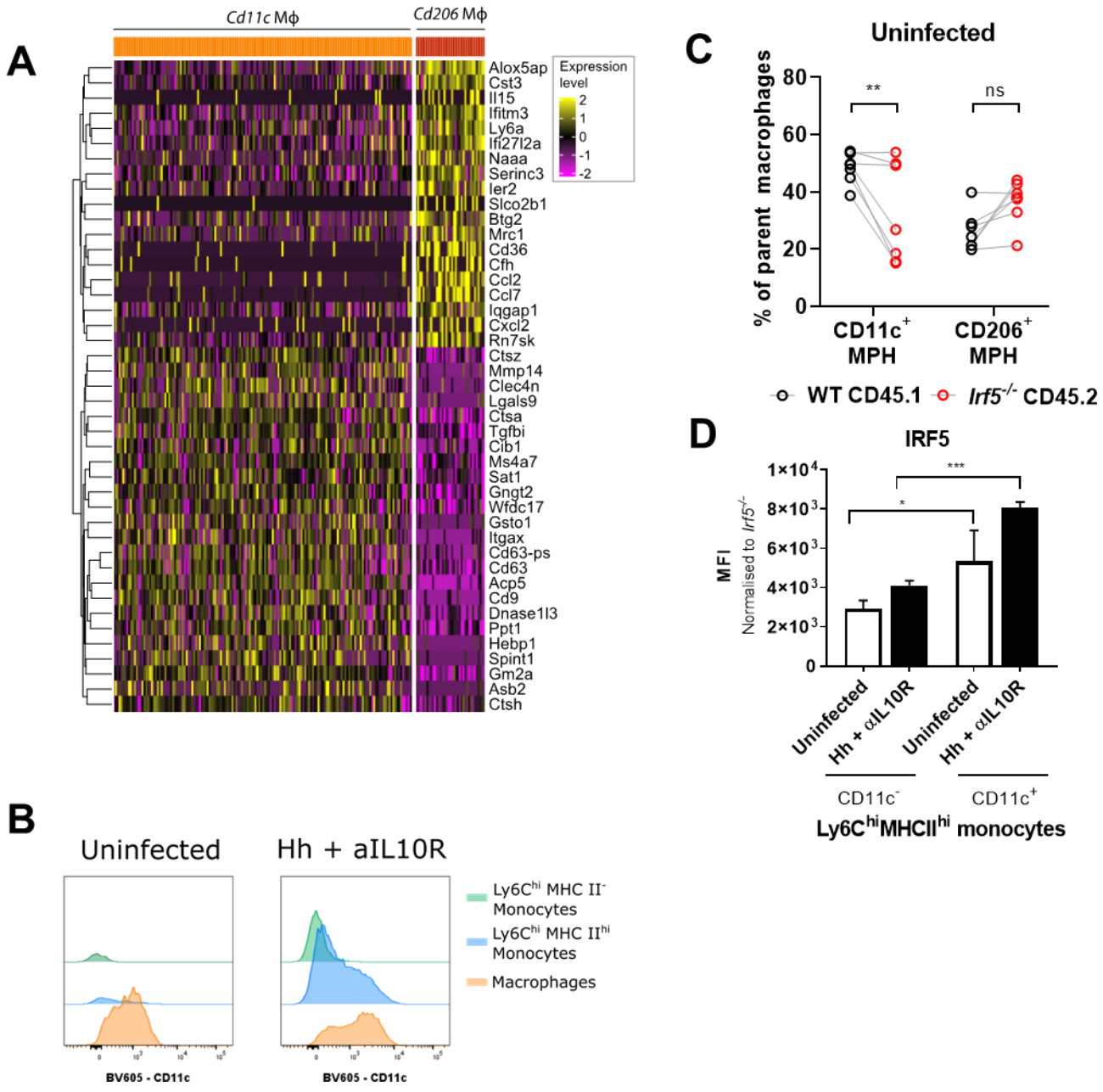


**Supplementary Figure S11: scRNA-seq: gene expression in *Cd11c* vs *Cd206* macrophages. A)** Heatmap of expression of selected genes in *Cd11c* and *Cd206* macrophages from the inflamed cLP of the MBMCs (see **Fig 5**). All of the genes shown were found to be differentially expressed between the *Cd11c* and *Cd206* clusters (Wilcoxon tests, BH adjusted p < 0.05). **B)** Cd11c protein surface expression levels on MNP populations. Representative histograms from 9 steady state and 12 d21 *Hh* + αIL10R experiments. **C)** The frequency of parent WT and *Irf5-/-* macrophages expressing CD11c or CD206 at steady state. Data from two independent experiments**. D)** IRF5 expression in $CD11c^+$ vs $CD11c^-$ Ly6ChiMHCII+ monocytes in MBMC assessed by intracellular flow cytometry. One representative experiment, uninfected n=3, Hh + αIL10R n=4.

**Table.1: List of antibodies used for surface staining**

| Epitope | Colour | Clone | Manufacturer | Cat # | Dilution |
|---|---|---|---|---|---|
| Annexin V | APC | N/A | Biolegend | 640919 | 1/20 |
| B220 | PerCP Cy5.5 | RA3-6B2 | eBio | 45-0452-82 | 1/200 |
| CD3 | PerCP Cy5.5 | 145-2C11 | Biolegend | 100328 | 1/200 |
| CD4 | BV605 | RM4-5 | Biolegend | 100547 | 1/400 |
| CD11b | V500 | M1/70 | BD | 562128 | 1/200 |
| CD11b | BV510 | M1/70 | Biolegend | 101245 | 1/200 |
| CD11c | BV605 | N418 | Biolegend | 117333 | 1/200 |
| CD11c | BV785 | N418 | Biolegend | 117335 | 1/200 |
| CD11c | PerCP-Cy5.5 | N418 | ThermoFisher | 45-0114-82 | 1/200 |
| CD16/32 | APC | 93 | eBioscience | 17-0161-82 | 1/200 |
| CD19 | Percp Cy5.5 | 6D5 | Biolegend | 115533 | 1/200 |
| CD31 | PE | MEC13.3 | Biolegend | 102507 | 1/200 |
| CD34 | FITC | RAM34 | BD | 553733 | 1/200 |
| CD34 | Biotin | RAM34 | ThermoFisher | 13-0341-82 | 1/200 |
| CD45 | V500 | 30-F11 | BD | 561487 | 1/400 |
| CD45 | BV650 | 30-F11 | BD | 563410 | 1/200 |
| CD45.1 | APC | A20 | eBioscience | 17-0453-82 | 1/200 |
| CD45.1 | BV650 | A20 | Biolegend | 110735 | 1/200 |
| CD45.1 | PE | A20 | eBio | 12-0453-82 | 1/200 |
| CD45.1 | PE Cy7 | A20 | eBioscience | 25-0453-82 | 1/200 |
| CD45.2 | AF700 | 104 | Biolegend | 109822 | 1/200 |
| CD45.2 | FITC | 104 | BD Pharmingen | 553772 | 1/200 |
| CD45.2 | PE | 104 | eBio | 12-0454-83 | 1/200 |
| CD45.2 | PE Cy7 | 104 | Biolegend | 109830 | 1/200 |
| CD45.2 | PerCP Cy5.5 | 104 | eBio | 45-0454-82 | 1/200 |
| CD64 | PE | X54-5/7.1 | Biolegend | 139303 | 1/100 |
| CD103 | PE | 2E7 | eBioscience | 12-1031-82 | 1/100 |
| CD138 | Percp Cy5.5 | 281-2 | Biolegend | 142509 | 1/200 |
| CD206 | APC | CO68L2 | Biolegend | 141708 | 1/100 |
| cKit | PB | 2B8 | Biolegend | 105820 | 1/200 |
| F4/80 | APC | BM8 | eBio | 17-4801-82 | 1/200 |
| F4/80 | PerCP-Cy5.5 | BM8 | eBioscience | 45-4801-82 | 1/100 |
| F4/80 | PE | BM8 | Biolegend | 123109 | 1/200 |
| F4/80 | PE/Dazzle 594 | BM8 | Biolegend | 123145 | 1/200 |
| FcεRIα | Percp Cy5.5 | MAR-1 | BioLegend | 134319 | 1/200 |
| Gp38 | PE-Cy7 | 8.1.1 | Biolegend | 127411 | 1/300 |
| IL-7Ra | PerCP Cy5.5 | A7R34 | Biolegend | 135021 | 1/200 |
| Ly6C | PE-Cy7 | HK1.4 | Biolegend | 128017 | 1/200 |
| Ly6C | BV785 | HK1.4 | Biolegend | 128041 | 1/300 |

| | | | | | |
|---|---|---|---|---|---|
| Ly6G | PerCP Cy5.5 | 1A8 | Biolegend | 127615 | 1/200 |
| Ly6G | PE-CF594 | 1A8 | BD | 562700 | 1/200 |
| MHC II | AF700 | M5/114.15.2 | eBioscience | 56-5321-80 | 1/200 |
| NK1.1 | PerCP Cy5.5 | PK136 | eBioscience | 45-5941-82 | 1/200 |
| Sca-1 | AF700 | D7 | eBio | 56-5981-82 | 1/200 |
| Siglec F | BV421 | E50-2440 | BD | 562681 | 1/200 |
| Siglec F | PE | E50-2440 | BD | 552126 | 1/200 |
| Streptavidin | BV605 | N/A | Biolegend | 405229 | 1/300 |
| TCRb | PerCP-Cy5.5 | H57-597 | eBioscience | 45-5961-82 | 1/200 |
| TCRb | AF700 | H57-597 | Biolegend | 109223 | 1/400 |
| Ter119 | PerCP-Cy5.5 | TER-119 | Biolegend | 116227 | 1/200 |

**Table.2: List of antibodies used for intracellular staining**

| Epitope | Colour | Clone | Manufacturer | Cat # | Dilution |
|---|---|---|---|---|---|
| Foxp3 | PE-eFluor 610 | FJK-15S | ThermoFisher | 61-5773-82 | 1/200 |
| Goat anti- rabbit (secondary ab) | AF488 | Polyclonal | Life Technologies | A-11008 | 1/300 |
| Il12p4/p70 | PE | C15.6 | BD | 562038 | 1/100 |
| IL-17A | FITC | 17B7 | eBioscience | 11-7177-81 | 1/200 |
| IFNg | APC | XMG1.2 | eBioscience | 17-7311-81 | 1/200 |
| IRF5 | N/A | Rabbit polyclonal | abcam | 21689 | 1/100 |
| Live/Dead | eF780 | N/A | ThermoFisher | 65-0865-14 | 1/1000 |
| TNFα | Pacific Blue | MP6-XT22 | Biolegend | 506318 | 1/100 |
| Pro-IL-1b | PE | NJTEN3 | ebioscience | 12F114-80 | 1/100 |